Table of Contents – Chapter VII

Page

1.6 Round-Robin NDT Trials 1

1.6.1 Trans Canada Pipe Weld Round-Robin PA Techniques 1
1.6.2. ExxonMobil Pipe Weld Evaluation 8
1.6.3 Thin-Walled Pipe 14

1.6.3.1 Lamb Wave Scans 15
1.6.3.2 PA AUT 20

1.6.4 UT Inspection for Service-Induced Fatigue Cracks 29

1.6.4.1 Fatigue Crack Samples W2 and W3 30

Tables

Table 1.6.1-1. Description of Ultrasonic Techniques Used 2

Table 1.6.2-1. Description of PA-AUT Techniques Used for Sample EM-001 9

Table 1.6.3-1. Description of Ultrasonic Techniques Used 20

Figures

Figure 1.6.1-1. Sample EWI-001 1

Figure 1.6.1-2. Comparison of PA4-64/21 (Left) and PA7-60/16 (Right) Results from Flaw 1408 3

Figure 1.6.1-3. PA4-64/21 US Scan 3

Figure 1.6.1-4. PA4-64/21 DS Scan 4

Figure 1.6.1-5. PA7-60/16 US Scan 4

Figure 1.6.1-6. PA7-60/16 DS Scan 5

Figure 1.6.1-7. PA7-60/9 US Scan 5

Figure 1.6.1-8. PA7-60/9 DS Scan 6

Figure 1.6.1-9. Weld EWI-001; AUT Flaw Height versus Destructive Flaw Height 7

Figure 1.6.1-10. Example of Flaws with High Width-to-Height Ratio 7

Figure 1.6.2-1. Sample EM-001 8

Table of Contents – Chapter VII (Continued)

Page

Figure 1.6.2-2. Comparison of PA4-64/21 (Left) and PA7-60/16 (Right) Results from Flaw 60 9

Figure 1.6.2-3. PA4-64/21 US Scan 10

Figure 1.6.2-4. PA4-64/21 DS Scan 10

Figure 1.6.2-5. PA7-60/16 US Scan 11

Figure 1.6.2-6. PA7-60/16 DS Scan 11

Figure 1.6.2-7. Polar View of PA7-60/16 US Scan 12

Figure 1.6.2-8. Weld EM-001; AUT Flaw Height versus Destructive Flaw Height 13

Figure 1.6.2-9. Example of Root Geometry Detected by PA AUT 13

Figure 1.6.3-1. Example of Decreased Inspection Coverage Caused by Probe Contacting Weld Cap 14

Figure 1.6.3-2. Drawing of Thin-Walled Sample as Designed 15

Figure 1.6.3-3. USLT 2000 System 16

Figure 1.6.3-4. Scanner Setup of Thin-Walled Pipe Sample 16

Figure 1.6.3-5. P/E Lamb Wave Initial Scan Data 17

Figure 1.6.3-6. P/E Lamb Wave Scan, Repeat #1 18

Figure 1.6.3-7. P/E Lamb Wave Scan, Repeat #2 18

Figure 1.6.3-8. Comparison of Lamb Wave Scan Data to Intended Flaw Locations 19

Figure 1.6.3-9. DPA4-24/24 US Scan Before Cap Removal 21

Figure 1.6.3-10. DPA4-24/24 DS Scan Before Cap Removal 21

Figure 1.6.3-11. PA10-32/16 US Scan Before Cap Removal 22

Figure 1.6.3-12. PA10-32/16 DS Scan Before Cap Removal 22

Figure 1.6.3-13. DPA4-24/24 US Scan After Cap Removal 23

Figure 1.6.3-14. DPA4-24/24 DS Scan After Cap Removal 23

Figure 1.6.3-15. PA10-32/16 US Scan After Cap Removal 24

Figure 1.6.3-16. PA10-32/16 DS Scan After Cap Removal 24

Table of Contents – Chapter VII (Continued)

Page

Figure 1.6.3-17. PA10-32/16 US Before Cap Removal 25

Figure 1.6.3-18. PA10-32/16 DS Before Cap Removal (First Leg) 25

Figure 1.6.3-19. PA10-32/16 DS Before Cap Removal (Third Leg) 26

Figure 1.6.3-20. PA10-32/16 US After Cap Removal 26

Figure 1.6.3-21. PA10-32/16 DS After Cap Removal 27

Figure 1.6.3-22. Metallography Results 28

Figure 1.6.4-1. Sound Beam Reflection from the Smooth Face of a Fatigue Crack Using the P/E Technique 29

Figure 1.6.4-2. Example of a 60-Degree Shear Wave Mode Converting to an L-Wave After Encountering a Fatigue Crack 29

Figure 1.6.4-3. Sound Beam Reflection from the Smooth Face of a Fatigue Crack Using the Tandem Pitch-Catch Technique 30

Figure 1.6.4-4. PA Sector Scan Showing Root Signals Caused by Root Geometry 31

Figure 1.6.4-5. Root Geometry of Weld W3 31

Figure 1.6.4-6. Crack W3-1 Showing Straight and Jagged Fracture Profiles 32

Figure 1.6.4-7. Flaw W3-1; UT Flaw Height Comparison to Metallographic Data 33

Figure 1.6.4-8. TOFD Scan Data from Flaw W3-1 33

Figure 1.6.4-9. Use of A-, B-, C-, D-, and S-scans to Visualize Flaw W3-1 34

Figure 1.6.4-10. Flaw W2-1; UT Flaw Height versus Actual Flaw Height 35

Figure 1.6.4-11. Flaw W3-1; UT Flaw Height versus Actual Flaw Height 36

Figure 1.6.4-12. Flaw W3-2; UT Flaw Height versus Actual Flaw Height 37

Figure 1.6.4-13. Sample W302-2 Showing OD Crack as Detected by Magnetic Particle Inspection 39

Figure 1.6.4-14. ID Corner Trap Signal from W302-2 Through-Wall Base Metal Crack When Using the P/E SE5-45 Technique 40

Figure 1.6.4-15. OD Corner Trap Signal from W302-2 Through-Wall Base Metal Crack When Using the P/E SE5-45 Technique 40

Figure 1.6.4-16. Merged D-Scan View of W302-2 Through-Wall Base Metal Crack When Using the P/E SE5-45 Technique 41

Table of Contents – Chapter VII

Page

Figure 1.6.4-17. Merged D-Scan View of W302-2 Through-Wall Base Metal Crack When Using the P/E SE5-60 Technique 41

Figure 1.6.4-18. ID Corner Trap Signal from W302-2 Through-Wall Base Metal Crack When Using the P/E SE5-60 Technique 42

Figure 1.6.4-19. OD Corner Trap Signal from W302-2 Through-Wall Base Metal Crack When Using the P/E SE5-60 Technique 42

Figure 1.6.4-20. Scan Results Using the PA7-60/17T-17R Tandem Technique on Flaw W302-2 43

Figure 1.6.4-21. Merged D-Scan View of W302-2 Through-Wall Base Metal Crack When Using the PA 7-MHz Tandem Pitch-Catch Technique 44

Figure 1.6.4-22. Multiple Signals from a Single Crack Using the Dual-PA Technique 45

Figure 1.6.4-23. Merged D-Scan View of W302-2 Through-Wall Base Metal Crack When Using the Dual-PA 4-MHz Pitch-Catch Technique 45

Figure 1.6.4-24. View of Merged Angle Data (45 to 70 Degrees) for Flaw W302-2 Using PA7-60/17 P/E Technique 46

1.6 Round-Robin NDT Trials

The results of several trails using different PA techniques applied on girth weld samples in a lab environment are presented in this section.

1.6.1 Trans Canada Pipe Weld Round-Robin PA Techniques

Large-diameter pipe with a relatively thin wall are common for cross-country pipelines. Consequently, AUT of girth welds in a large-diameter, thin-walled pipe were evaluated during this project. Pipe sections were provided to EWI by TransCanada for use during this portion of the project. The pipe, identified by EWI as EWI-001, was a 610-mm (24-in.)-diameter pipe having a 7.8-mm (0.31-in.) nominal wall thickness. The weld bevel was a V-groove having a 30-degree bevel angle. Sample EWI-001 is shown in Figure 1.6.1-1. Upon receipt of the material, EWI fabricated two girth welds containing intentional flaws. The initial weld was a practice piece used to establish welding parameters for creating flaws. After the practice piece was completed and the flaws verified by use of radiography, a second weld was fabricated for use as the primary sample for evaluation by AUT.

Figure 1.6.1-1. Sample EWI-001

After fabrication of the girth welds, EWI performed PA-AUT on both the practice piece and the primary sample. Both welds were tested using the PA4-64/21 and PA7-60/16 techniques shown in Table 1.6.1-1. The primary sample weld was also tested using the PA7-60/9 technique described in Table 1.6.1-1. The welds were scanned from both the US and DS sides. In order to obtain maximum through-wall coverage of the weld, the beam exit point on the wedge was moved as close as possible to the front of the wedge. This was accomplished by

selecting the upper most elements of each probe in the focal laws for each probe. Although the PA4-64/21 and PA7-60/16 techniques used different numbers of elements, the aperture sizes were similar.

Table 1.6.1-1. Description of Ultrasonic Techniques Used

Technique Designation	Freq. (MHz)	No. of Total Elements	No. of Elements Used	Element Dimensions (mm)	Beam Angle (degrees)
PA4-64/21	4	64	21	0.7×15	45-70 shear
PA7-60/16	7.5	60	16	0.9×10	45-70 shear
PA7-60/9	7.5	60	9	0.9×10	45-70 shear

The initial 7-MHz scans were performed using 16 elements with a focal depth of 20 mm (0.8 in.). Later, a second 7-MHz scan PA7-60/9 technique was performed using nine elements with a 11-mm (0.4-in.) focal depth in an attempt to move the beam exit point on the wedge closer to the weld and to electronically focus at approximately mid-wall on the second leg. Because of the relatively thin wall of this pipe, it was thought that this technique might provide better through-wall coverage of the weld.

A raster scan pattern was used to collect data at 2.0-mm (0.08-in.) intervals in the scan direction and 4.0-mm (0.16-in.) intervals in the index direction. In addition, the scan direction for all scans was parallel to the pipe axis and the index direction was parallel to the pipe circumference. Figures 1.6.1-2 through 1.6.1-6 show the scan results for both the PA4-64/21 and PA7-60/16 techniques.

The reference calibration gain for both probes was established using a 19.1-mm (0.75-in.)-deep SDH having a 1.2-mm (0.047-in.) diameter. Using a refracted shear wave angle of 53 degrees the gain was adjusted to produce an amplitude of 80% of FSH from the calibration hole. Scanning gain for the PA 4 probe was 6 dB above the calibration gain. Scanning gain for the PA 7.5 probe was 10 dB above the calibration gain. Wedge noise in the PA 4 probe prevented the use of a higher scanning gain.

While both the PA7-60/16 and the PA4-64/21 techniques detected the weld flaws, the PA7-60/16 technique detected the flaws slightly better than the PA4-64/21 technique and provided a better defined signal for flaw sizing purposes. The differences in detection capabilities of each technique can be seen in Figures 1.6.1-2 through 1.6.1-6. The PA7-60/9 scans did not improve the detectability or resolution. In fact, the reduction in aperture size from 16 elements to 9 elements significantly reduced the gain. Attempts to improve the signal amplitude by adding

additional gain resulted in an unacceptable increase in noise level. The reduced aperture size did allow the beam exit point on the wedge to shift closer to the weld; however, at angles above 55 degrees the beam exit point was beyond the front of the wedge resulting in loss of data at higher inspection angles. Test results for the PA7-60/9 technique are shown in Figures 1.6.1-7 and 1.6.1-8. After scanning, a total of seven locations were selected from Sample EWI-001 for metallographic cross sectioning.

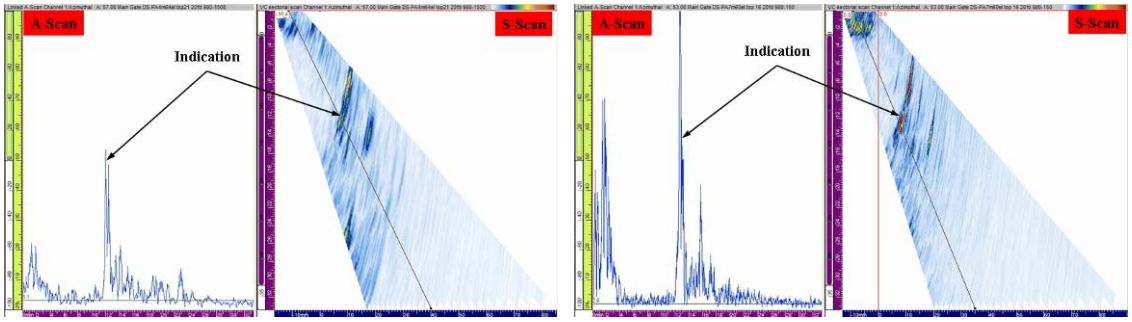

Figure 1.6.1-2. Comparison of PA4-64/21 (Left) and PA7-60/16 (Right) Results from Flaw 1408

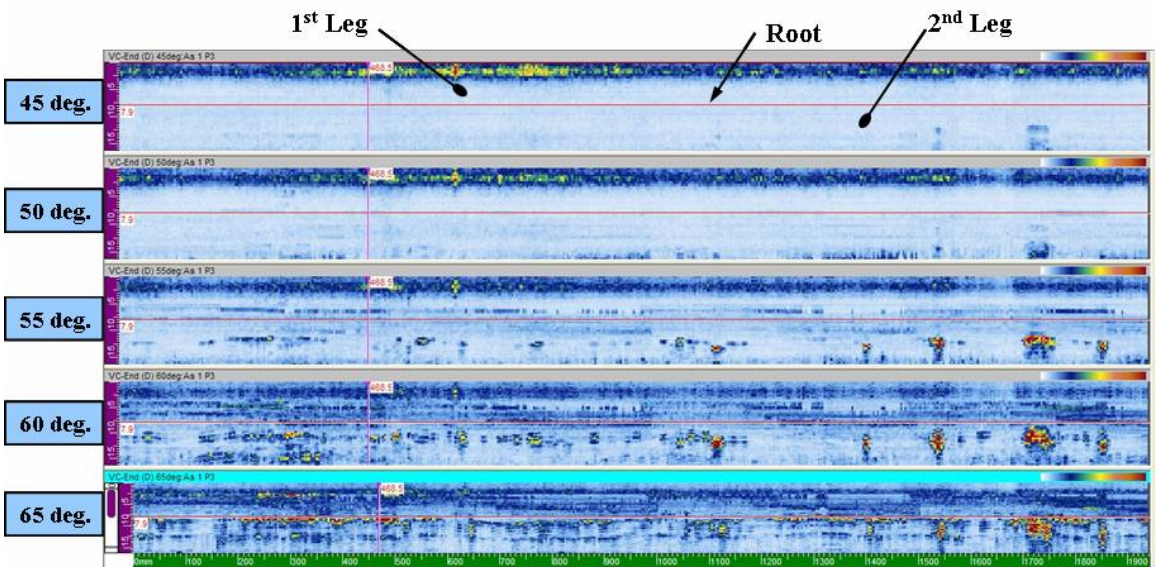

Figure 1.6.1-3. PA4-64/21 US Scan

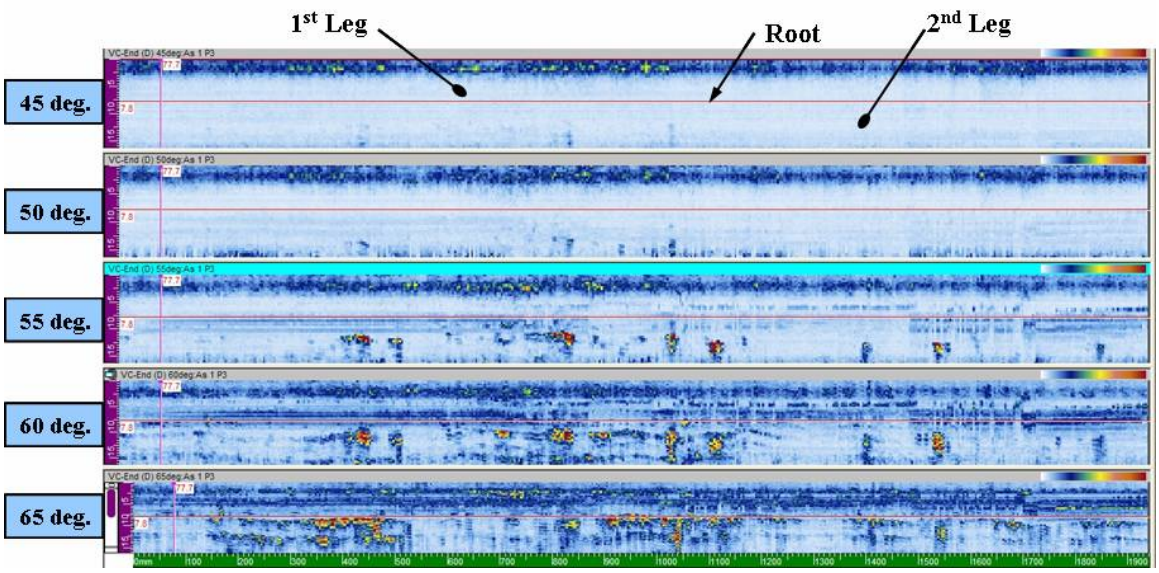

Figure 1.6.1-4. PA4-64/21 DS Scan

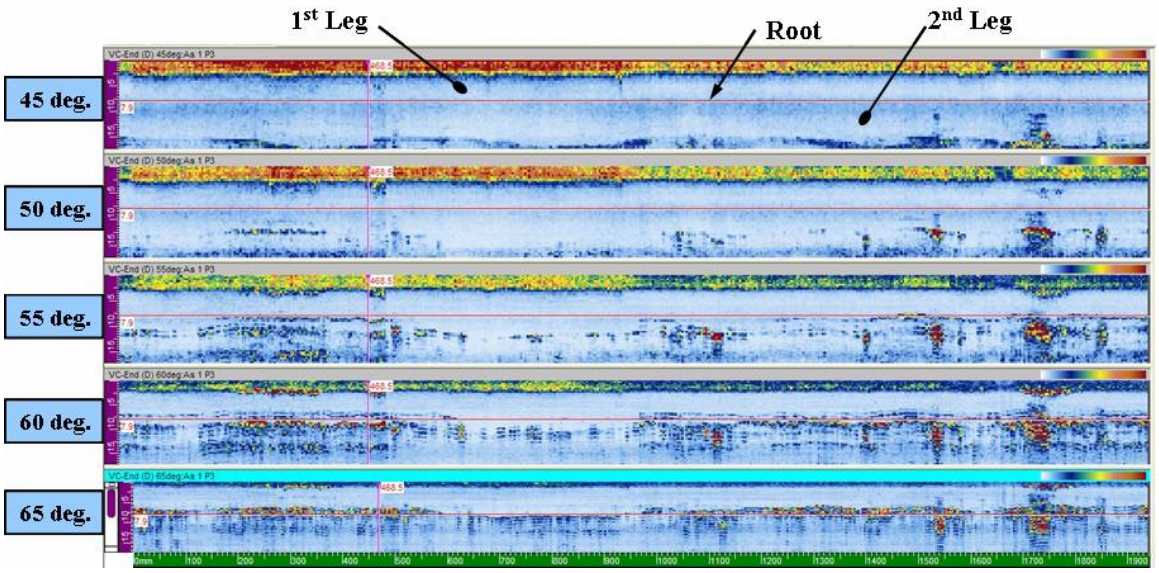

Figure 1.6.1-5. PA7-60/16 US Scan

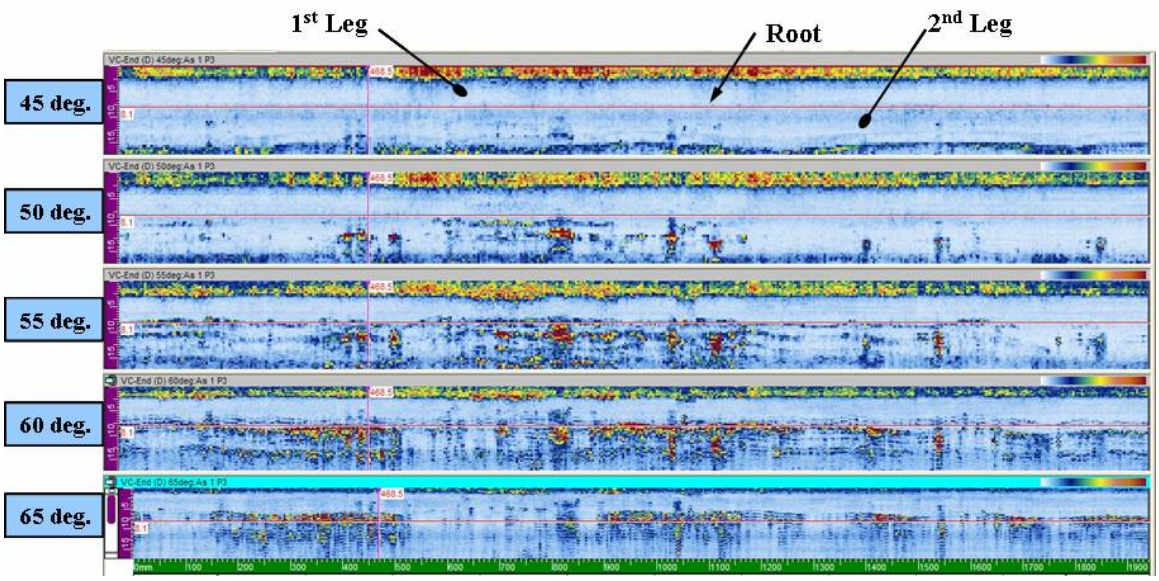

Figure 1.6.1-6. PA7-60/16 DS Scan

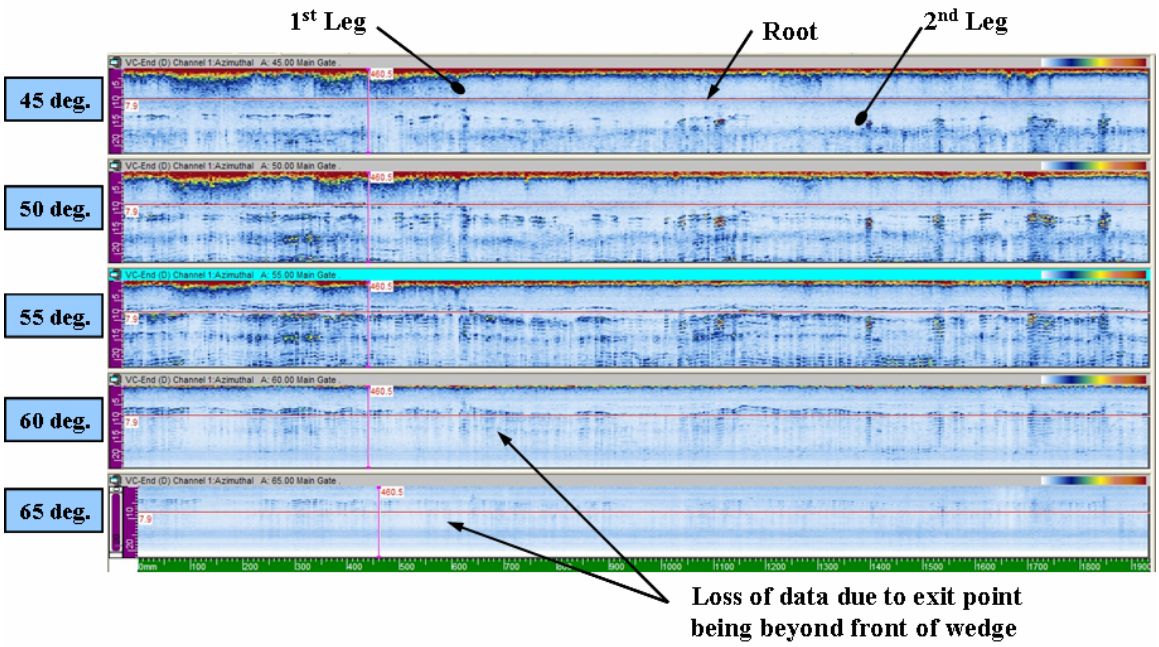

Figure 1.6.1-7. PA7-60/9 US Scan

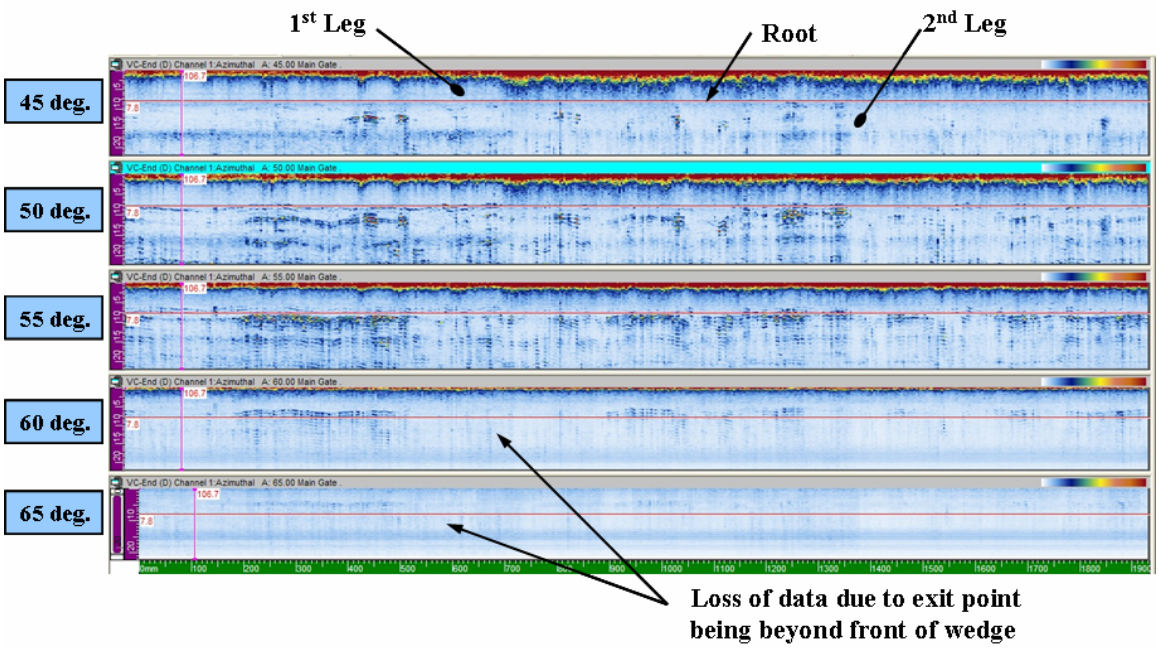

Figure 1.6.1-8. PA7-60/9 DS Scan

The scan axis data was merged together for five different angles (45, 50, 55, 60, and 65 degrees) and displayed for the entire weld length (Figures 1.6.1-3 and 1.6.1-8). This allowed flaws to be quickly viewed on the first and second legs at all five angles along the weld length. This viewing technique also provided quick analysis of the through-wall extension and length of each flaw. A more detailed analysis of the flaw height of each flaw selected for metallographic cross sectioning was performed using the S-scan display (Figure 1.6.1-2). A total of seven locations were selected for metallographic cross sectioning. Appendix A1.6.1 shows A- and S-scan images from data collected using the two PA techniques on the seven flaws selected for cross sectioning. Since the scans from the PA7 technique were better defined, this scan data was the only data used for AUT sizing. A comparison of the PA data to the metallographic cross section results are shown in Figure 1.6.1-9.

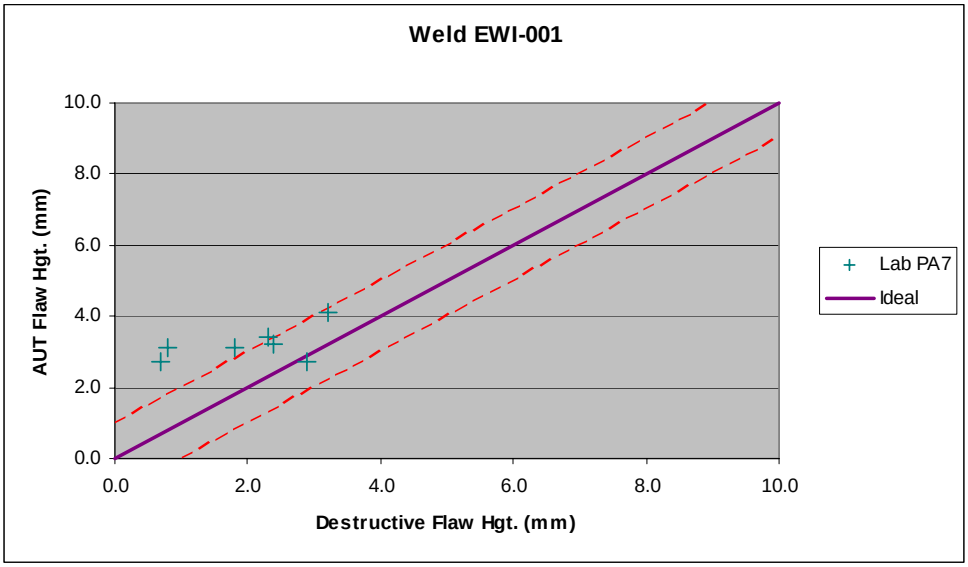

Figure 1.6.1-9. Weld EWI-001; AUT Flaw Height versus Destructive Flaw Height

The PA-AUT flaw wall height measurements for Weld EWI-001 were oversized when compared to the destructive flaw height measurements. Most of the flaws in Weld EWI-001 were more volumetric than planar in shape. The width-to-height ratio of the flaws was typically 1:1 or greater as shown in Figure 1.6.1-10. This resulted in a strong reflected signal from the flaws making the signal echodynamic larger which also made the through-wall height appear larger.

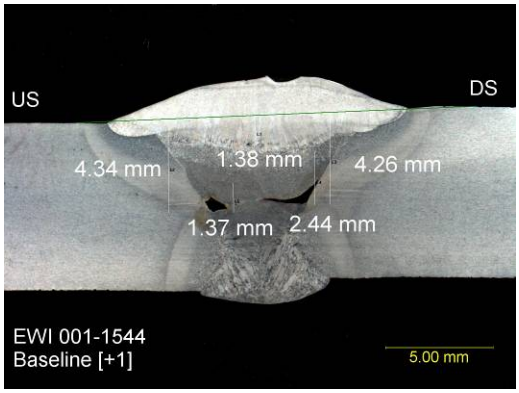

Figure 1.6.1-10. Example of Flaws with High Width-to-Height Ratio

1.6.2. ExxonMobil Pipe Weld Evaluation

A pipe girth weld was furnished to EWI by ExxonMobil for the purpose of detecting and sizing unknown flaws in the weld. The pipe, identified by EWI as EM-001, was a 32.4-cm (12.75-in.)-diameter pipe having an 11.4-mm (0.45-in.) nominal wall thickness. The weld bevel was a V-groove having a 30-degree bevel angle. The flaws in Sample EM-001 were weld flaws fabricated by varying the welding parameters during the welding process. Sample EM-001 is shown in Figure 1.6.2-1.

Figure 1.6.2-1. Sample EM-001

Upon receipt of the pipe weld, EWI performed PA AUT using the two PA techniques described in Table 1.6.2-1. The weld was scanned from both the US and DS sides of the weld using the two PA UT techniques. In order to obtain maximum through-wall coverage of the weld, the beam exit point on the wedge was moved as close as possible to the front of the wedge. This was accomplished by selecting the upper most elements of each probe in the focal laws. Although the number of elements used for each technique was different, the aperture sizes were similar. Element groupings of 14 to 21 elements and electronic focal depths of 12 to 25 mm (0.5 to 1.0 in.) were tried in order to optimize the overall UT signal response from the weld.

A raster scan pattern was used to collect data at 2.0-mm (0.08-in.) intervals in the scan direction and 4.0-mm (0.16-in.) intervals in the index direction. For all scans the scan direction was parallel to the pipe axis and the index direction was parallel to the pipe circumference. Figures 1.6.2-3 through 1.6.2-6 show the scan results for both the PA4-64/21 and PA7-60/16 techniques.

The reference calibration gain for both probes was established using a 25.4-mm-deep SDH having a diameter of 1.2 mm. Using a refracted shear wave angle of 53 degrees the gain was adjusted to produce an amplitude of 80% of FSH from the calibration hole. Scanning gain for the PA 4 probe was 6 dB above the calibration gain. Scanning gain for the PA 7.5 probe was 10 dB above the calibration gain. Wedge noise in the PA 4 probe prevented the use of a higher scanning gain.

Table 1.6.2-1. Description of PA-AUT Techniques Used for Sample EM-001

Technique Designation	Freq. (MHz)	No. of Total Elements	No. of Elements Used	Element Dimensions (mm)	Beam Angle (degrees)
PA4-64/21	4	64	21	0.7×15	45-70 shear
PA7-60/16	7.5	60	16	0.9×10	45-70 shear

While both techniques detected the weld flaws reasonably well, the PA7-60/16 technique detected the weld flaws slightly better than the PA4-64/21 technique and provided a more defined signal for flaw sizing purposes. The differences in detection capabilities of each technique can be seen in Figures 1.6.2-2 through 1.6.2-6.

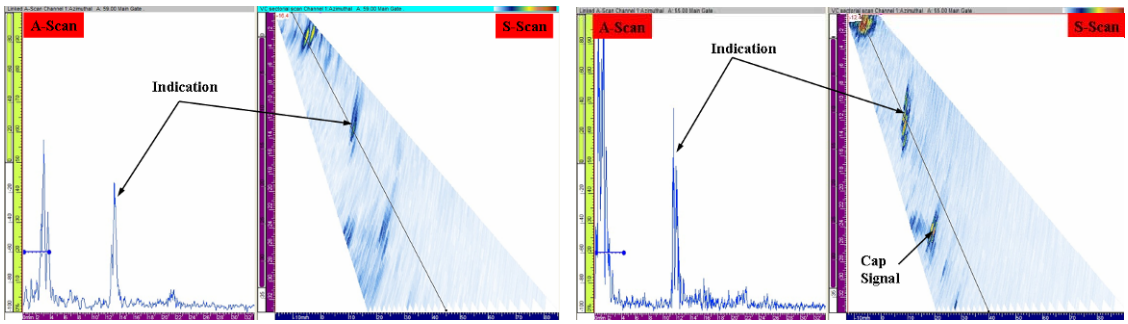

Figure 1.6.2-2. Comparison of PA4-64/21 (Left) and PA7-60/16 (Right) Results from Flaw 60

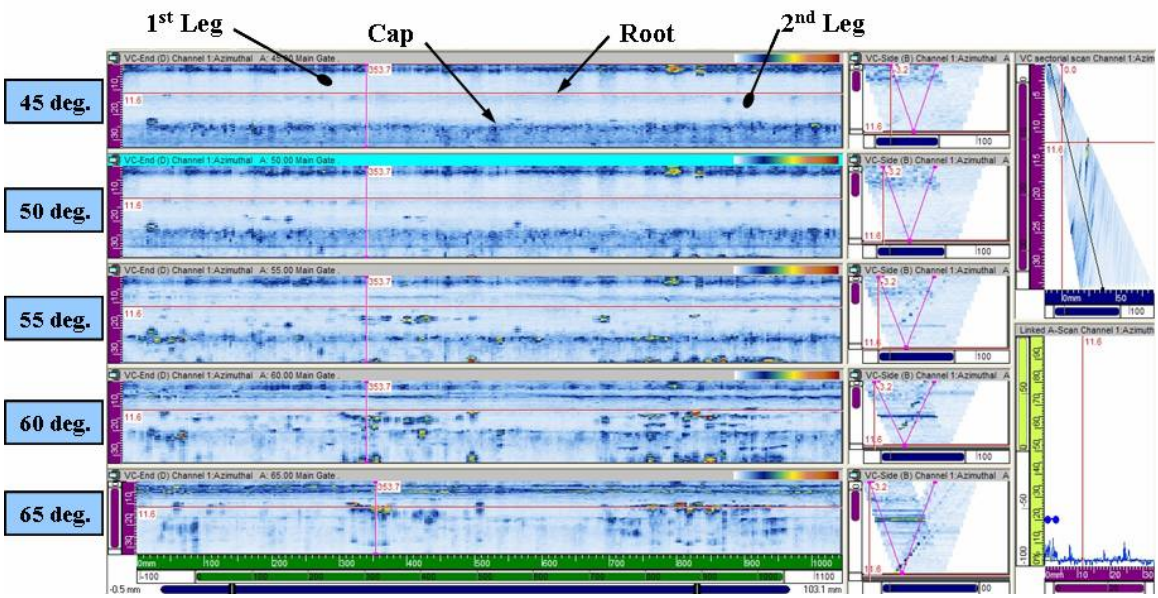

Figure 1.6.2-3. PA4-64/21 US Scan

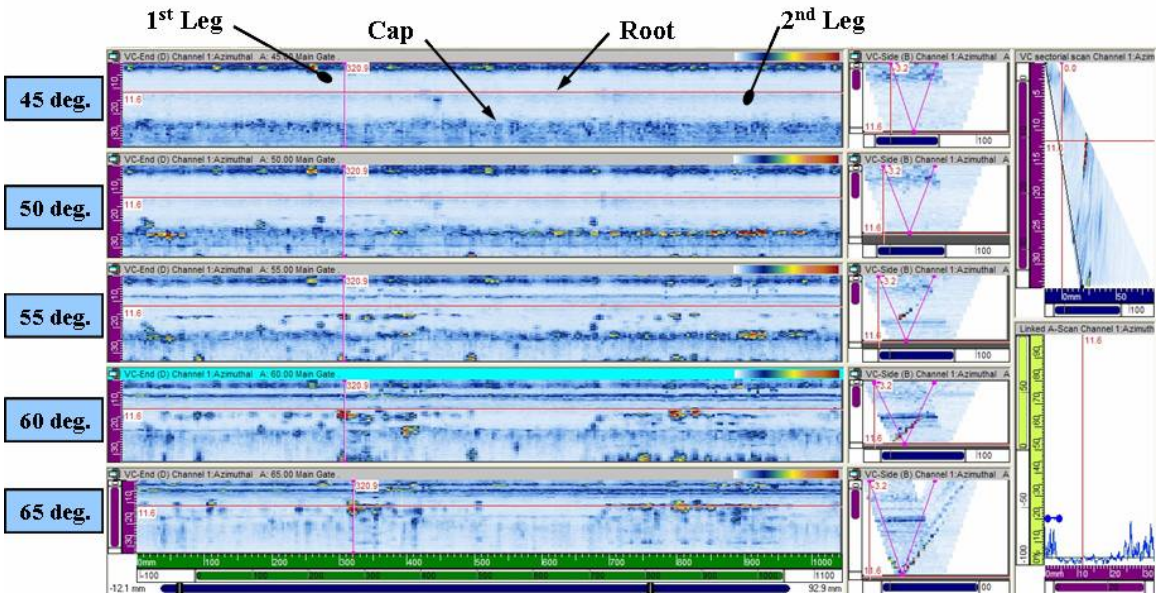

Figure 1.6.2-4. PA4-64/21 DS Scan

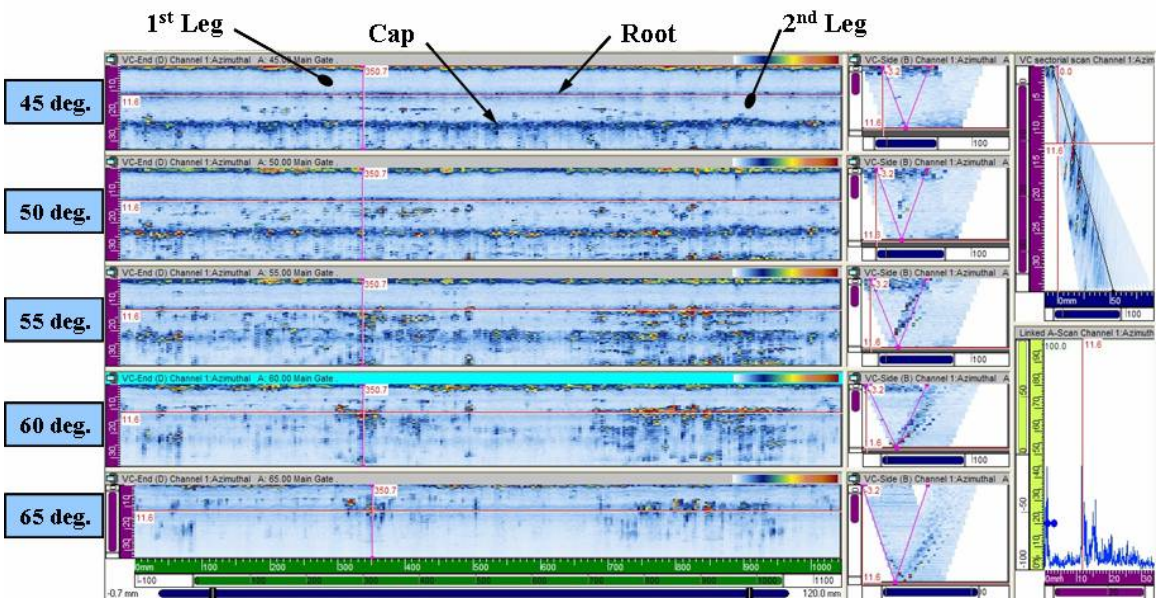

Figure 1.6.2-5. PA7-60/16 US Scan

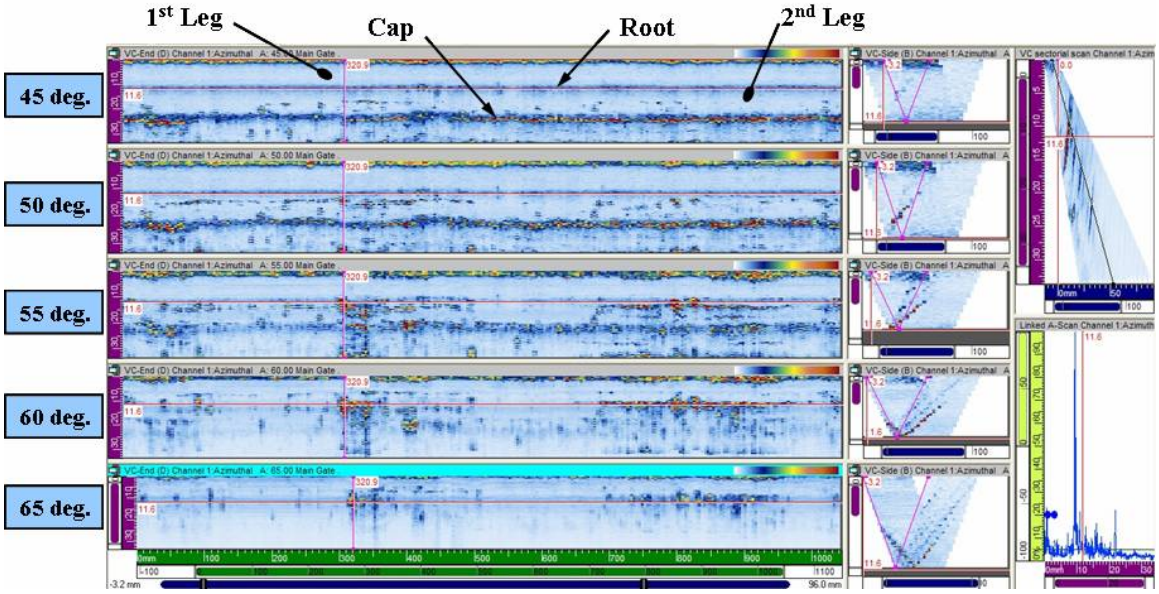

Figure 1.6.2-6. PA7-60/16 DS Scan

For viewing purposes, the scan axis data was merged together for five different angles (45, 50, 55, 60, and 65 degrees) and displayed for the entire weld length (Figures 1.6.2-3 through 1.6.2-6). This allowed flaws to be quickly viewed on the first and first legs at all five angles along the weld length. This viewing technique also provided quick analysis of the through-wall extension and length of each flaw. The use of polar views also helped visualize the location and size of flaws. An example of a polar view for the PA7-60/16 US scan is shown in Figure 1.6.2-7.

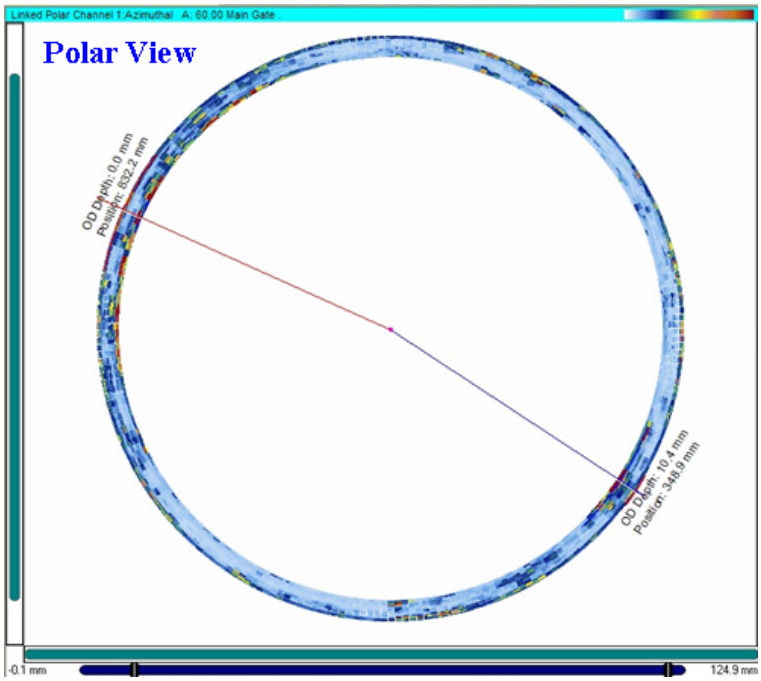

Figure 1.6.2-7. Polar View of PA7-60/16 US Scan

A more detailed analysis of the flaw height for each flaw selected for metallographic cross sectioning was performed using the S-scan display (Figure 1.6.2-2). A total of 13 locations were selected for metallographic cross sectioning. Appendix A1.6.2 shows A- and S-scan images from data collected using the two PA techniques on the 13 flaws selected for cross sectioning. Since the scans from the PA7 technique were better defined, this scan data was the only data used for AUT sizing. A comparison of the PA data to the metallographic cross section results are shown in Figure 1.6.2-8.

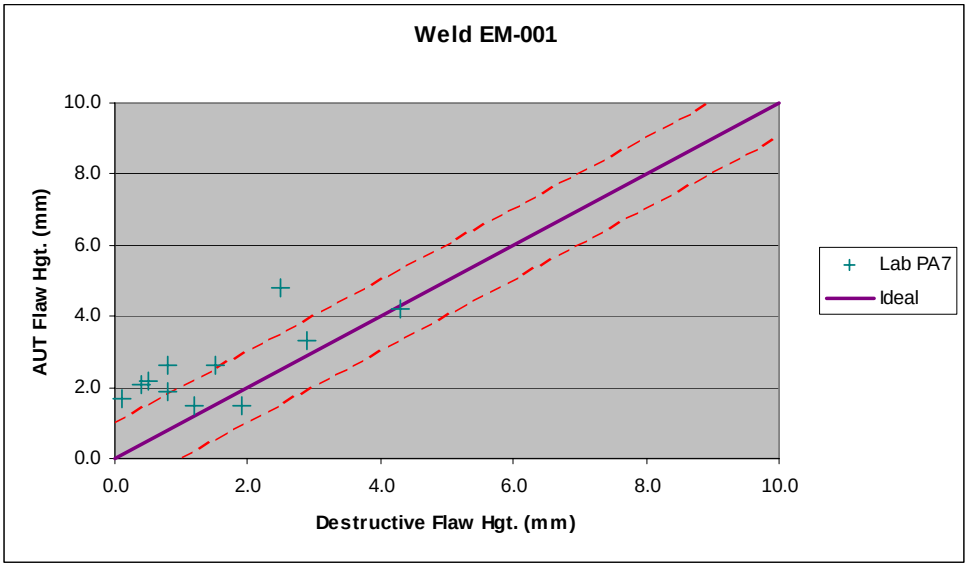

Figure 1.6.2-8. Weld EM-001; AUT Flaw Height versus Destructive Flaw Height

A comparison of the PA-AUT flaw height sizing shows that when the flaw height was less than 2 mm (0.08 in.) the flaw was oversized. One explanation for this is the fact that the sound beam in the through-wall dimension was approximately 2 to 3 mm (0.08 to 0.12 in.). Four of the flaws reported by the PA AUT were not found during metallographic cross sectioning. All four were reported as root flaws and were possibly caused by root geometry. Figure 1.6.2-9 shows a location on Weld EM-001 where root geometry was possibly misidentified as a flaw.

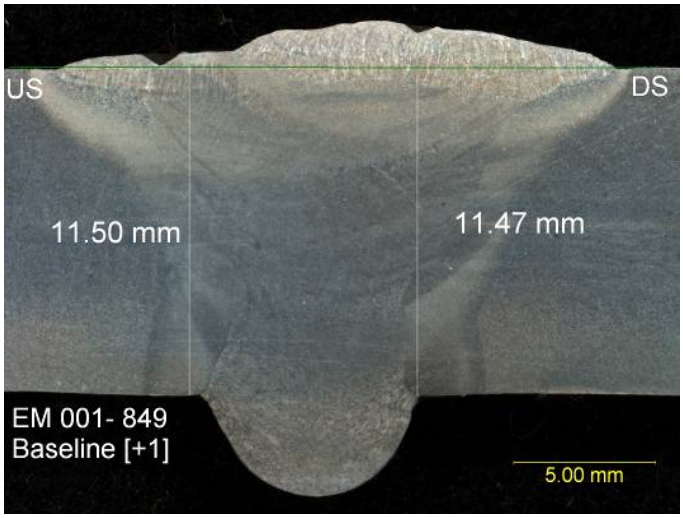

Figure 1.6.2-9. Example of Root Geometry Detected by PA AUT

1.6.3 Thin-Walled Pipe

Obtaining a good UT inspection of thin-walled pipe is often challenging. This is primarily due to a combination of probe dimensions, pipe wall thickness and weld cap width. A wide weld cap can prevent the probe from getting close enough for full inspection coverage as shown in Figure 1.6.3-1. Inspection coverage can be improved by grinding the weld cap, but often this is an unacceptable option because of cost or schedule restrictions.

During this project PA-AUT techniques and Lamb wave UT techniques were used to scan a thin-walled pipe sample containing implanted flaws. The various techniques were evaluated to determine their effectiveness for detecting girth weld flaws in thin-walled pipe. The sample was a 168-mm (8.63-in.)-diameter pipe with a nominal wall thickness of approximately 4.5 mm (0.18 in.). The design called for four flaws to be implanted in the sample (two LOF flaws and two cracks); however, during metallographic cross sectioning it was determined that only the two cracks were present. Figure 1.6.3-2 shows the design drawing for the thin wall sample.

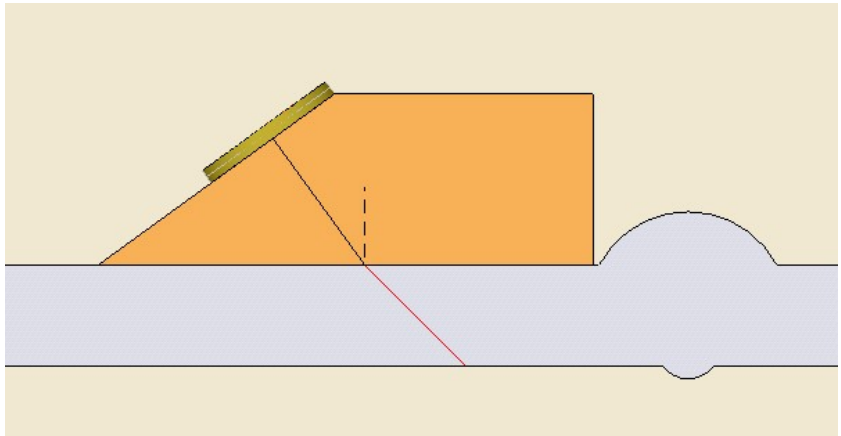

Figure 1.6.3-1. Example of Decreased Inspection Coverage Caused by Probe Contacting Weld Cap

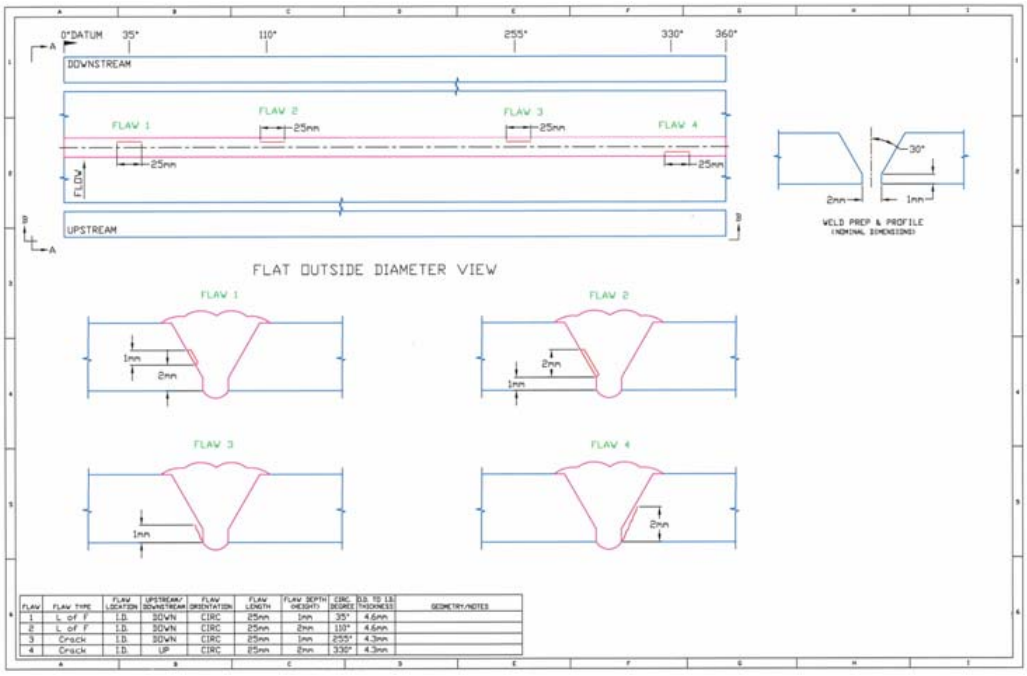

Figure 1.6.3-2. Drawing of Thin-Walled Sample as Designed

1.6.3.1 Lamb Wave Scans

The thin-walled sample was scanned using a Lamb wave technique where sound energy is transmitted through the weld in a P/E arrangement. The scan was performed using a GE Inspection Technologies USLT 2000 ultrasonic system connected to a specially designed scanner. The test instrument and scanner are shown in Figure 1.6.3-3. The USLT 2000 module is an independent unit which fits into the framework of a desktop or laptop computer. The Lamb wave-based scanner used for these scans consisted of a single-element transducer with a 4-MHz center frequency and a 45-degree wedge angle. The transducer was mounted inside a wheel assembly which was coupled to the pipe using a proprietary dry-coupling material on the surface of the wheel.

Initially, a pitch-catch technique was considered with the pulsing transducer on one side of the weld and the receiving probe on the other side of the weld. However, the pitch-catch technique proved to be inadequate due to the relative small flaw dimensions. Consequently, the P/E technique, using just one probe, was considered the best option.

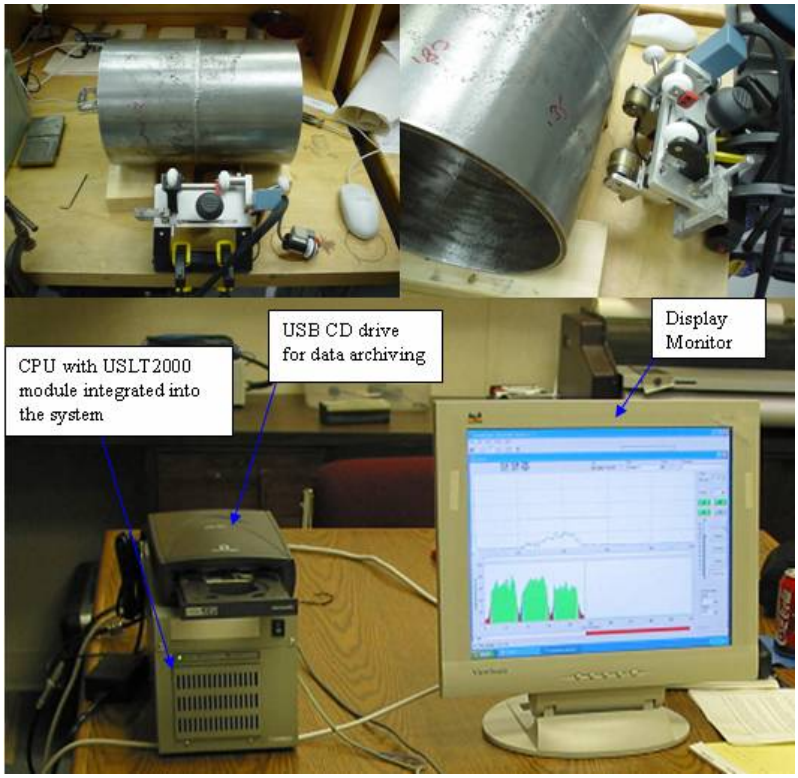

Figure 1.6.3-3. USLT 2000 System

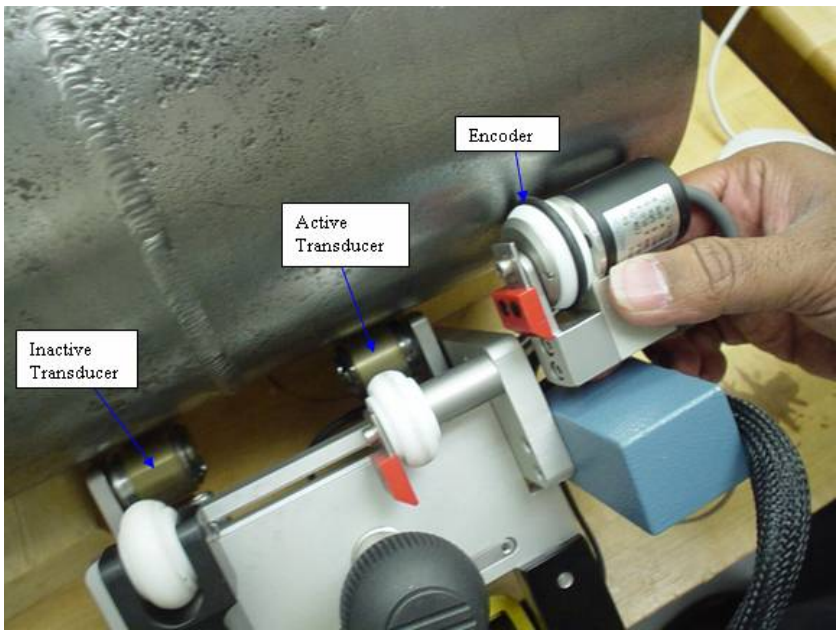

Figure 1.6.3-4. Scanner Setup of Thin-Walled Pipe Sample

The scan was setup for P/E as shown in Figure 1.6.3-4. No calibration sample was available for use with this equipment so the system was setup using the backwall of the pipe. The scan length was set for 700 mm (27.6 in.) which provided full coverage of the weld length (pipe circumference) with approximately 10-mm (0.39-in.) overlap. An initial scan was performed and then two additional repeat scans were performed using the same instrument settings to look at test variability. The scan results are shown in the screen capture images in Figures 1.6.3-5 through 1.6.3-7.

Figure 1.6.3-5. P/E Lamb Wave Initial Scan Data

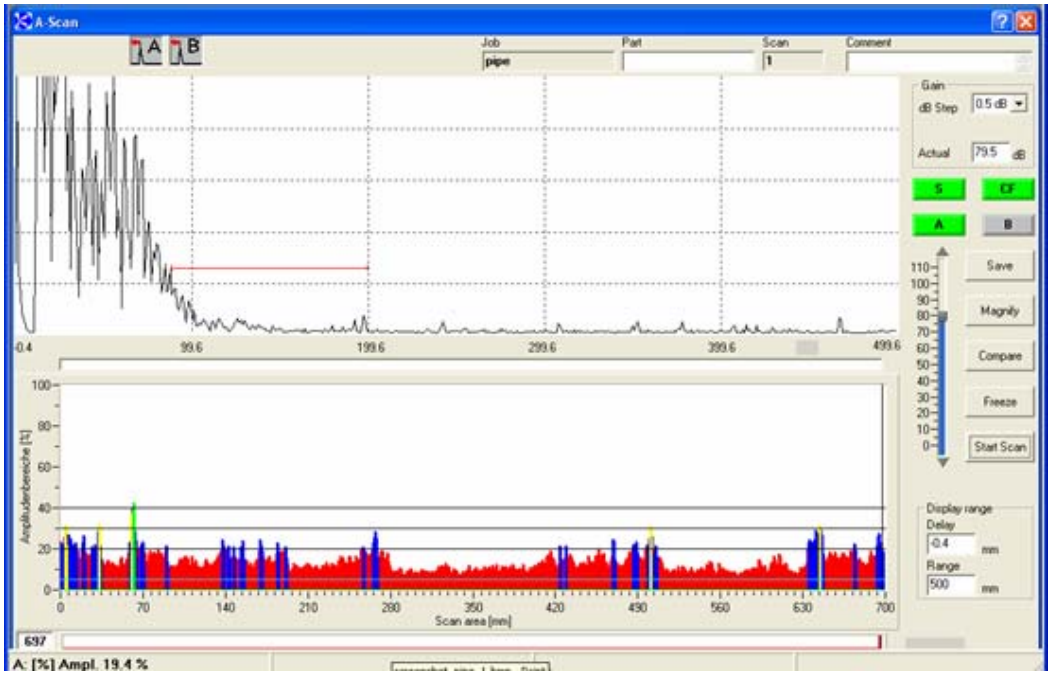

Figure 1.6.3-6. P/E Lamb Wave Scan, Repeat #1

Figure 1.6.3-7. P/E Lamb Wave Scan, Repeat #2

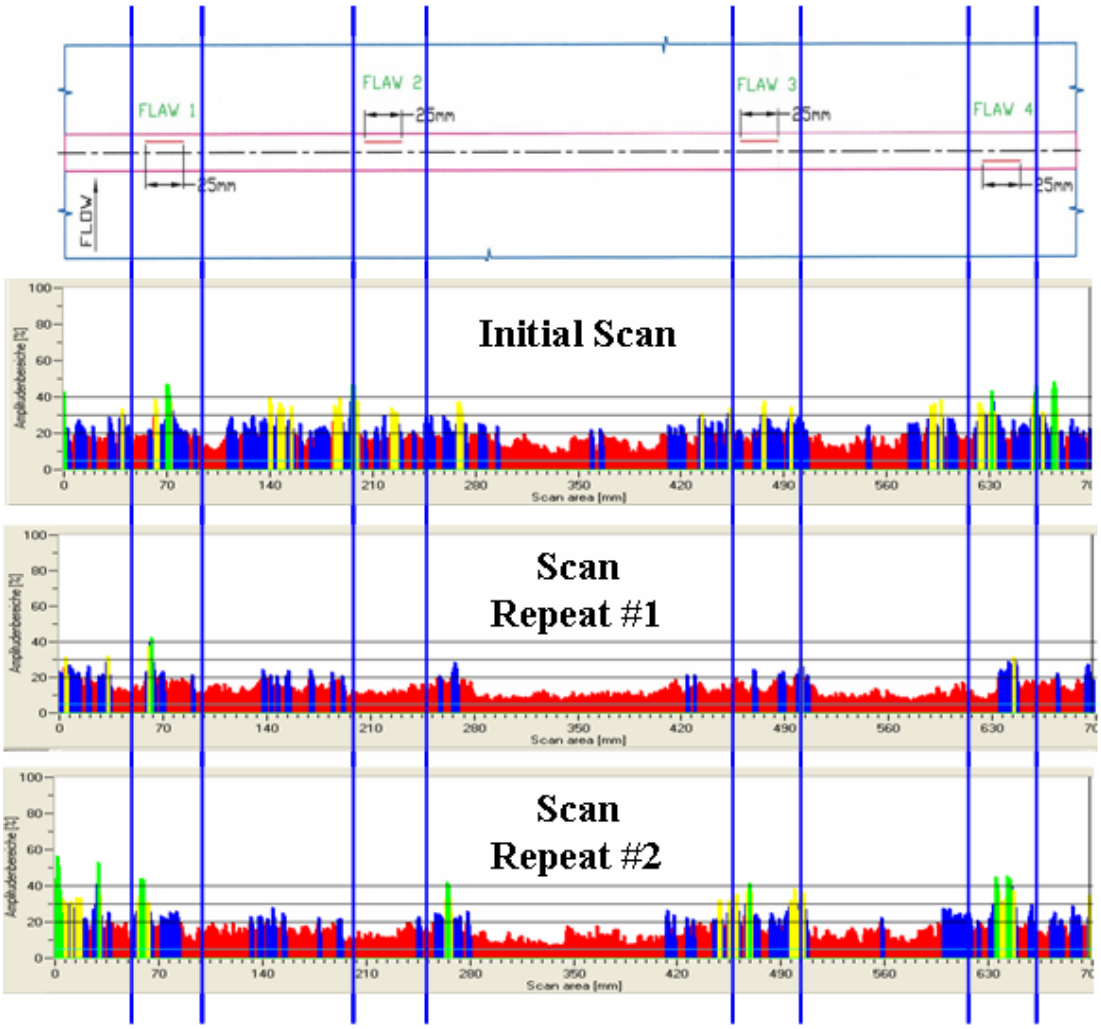

Figure 1.6.3-8. Comparison of Lamb Wave Scan Data to Intended Flaw Locations

While the data acquisition and instrumentation performed well, the scanner and probe used for these scans was originally designed for scanning thin, flat material and was not optimized for scanning pipe girth welds. The mismatch in the pipe fit up was detected and resulted in the background noise level being relatively high. Figure 1.6.3-8 shows that the reflected signal level increased in areas where flaws were located; however, the detection capabilities appeared to be minimal with the current design. It is possible that by redesigning the scanner and probes, this technology could be useful for inspection of girth welds in thin wall pipe; however, this was beyond the scope of this project.

1.6.3.2 PA AUT

The thin-walled sample was also evaluated using PA AUT techniques. These scans were performed with the weld cap present and after the weld cap was removed by grinding. Two shear wave PA techniques were evaluated. The first was a dual-PA pitch-catch technique using 4-MHz, 24-element probes, and the second was a P/E PA technique using a 10-MHz, 32-element probe. The PA techniques are summarized in Table 1.6.3-1.

Table 1.6.3-1. Description of Ultrasonic Techniques Used

Technique Designation	Freq. (MHz)	No. of Total Elements	No. of Elements Used	Element Dimensions (mm)	Beam Angle (degrees)
DPA4-24/24	4	24	24	0.7 × 8	45-70 shear
PA10-32/16	10	32	16	0.2 × 7	45-70 shear

The weld was scanned from the US and DS sides using both the DPA4-24/24 and the PA10-32/16 techniques. Scans were done before and after removal of the weld cap. For both techniques the beam was electronically focused at approximately mid-wall on the second leg. The reference calibration gain for both probes was established using a 10.7-mm (0.50-in.)-deep SDH having a 1.2-mm (0.047-in.) diameter. Using a refracted shear wave angle of 53 degrees, the gain was adjusted to produce an amplitude of 80% of FSH from the calibration hole. Scanning gain for both probes was 10 to 12 dB above the calibration gain. A raster scan pattern was used to collect data at 2.0-mm (0.08-in.) intervals in the scan direction and 4.0-mm (0.16-in.) intervals in the index direction. The scan direction for all scans was parallel to the pipe axis and the index direction was parallel to the pipe circumference.

Figures 1.6.3-9 through 1.6.3-12 show the scan results for both techniques prior to removal of the weld cap and Figures 1.6.3-13 through 1.6.3-16 show the scan results after weld cap removal.

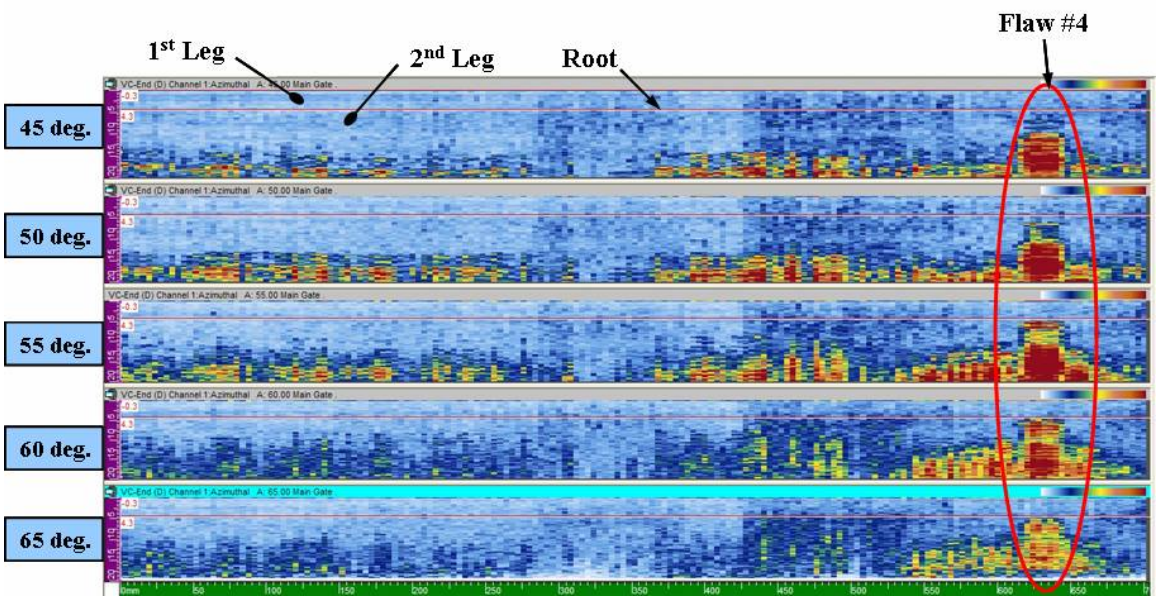

Figure 1.6.3-9. DPA4-24/24 US Scan Before Cap Removal

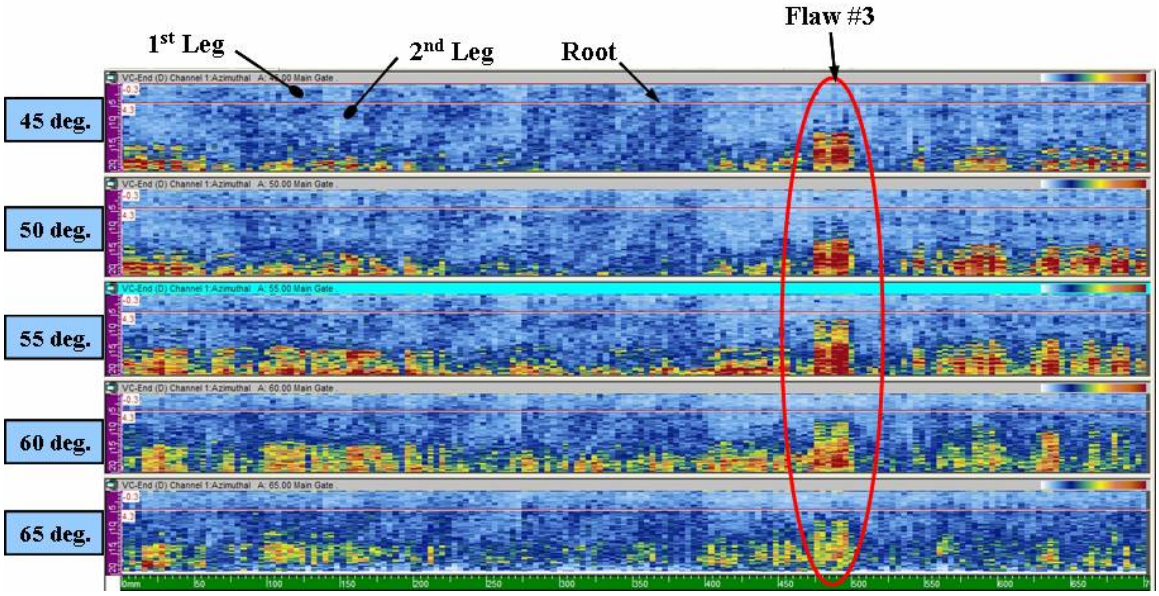

Figure 1.6.3-10. DPA4-24/24 DS Scan Before Cap Removal

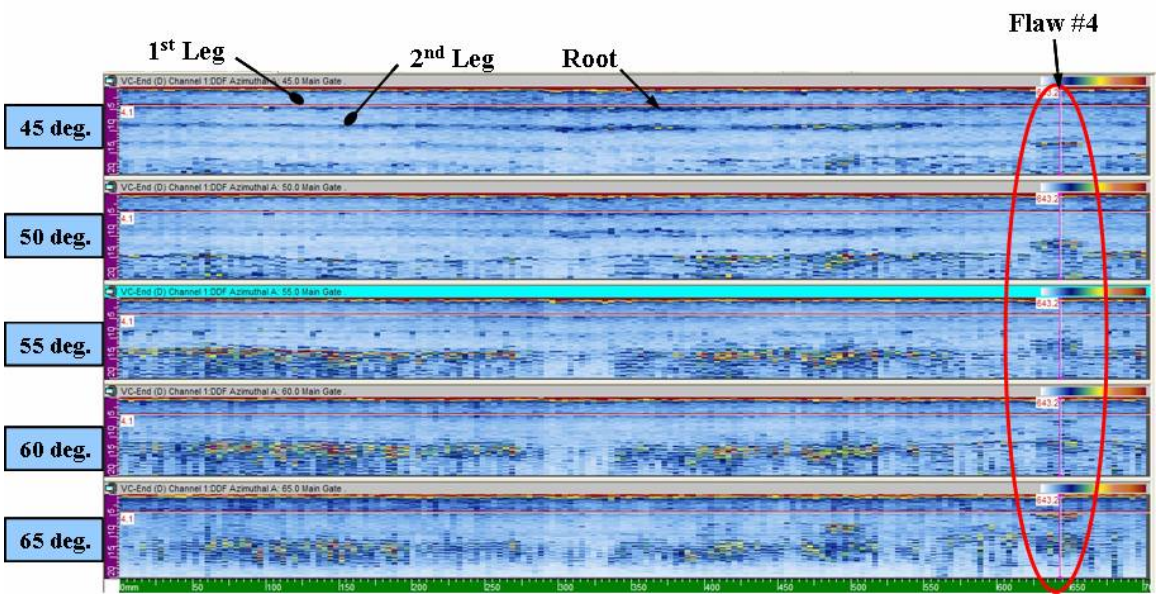

Figure 1.6.3-11. PA10-32/16 US Scan Before Cap Removal

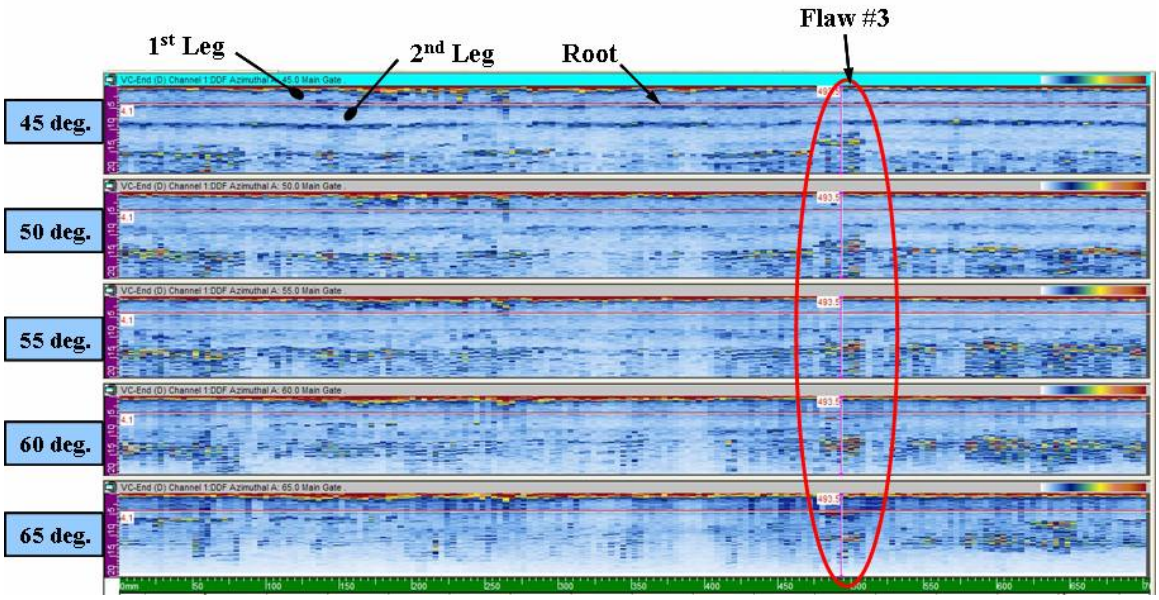

Figure 1.6.3-12. PA10-32/16 DS Scan Before Cap Removal

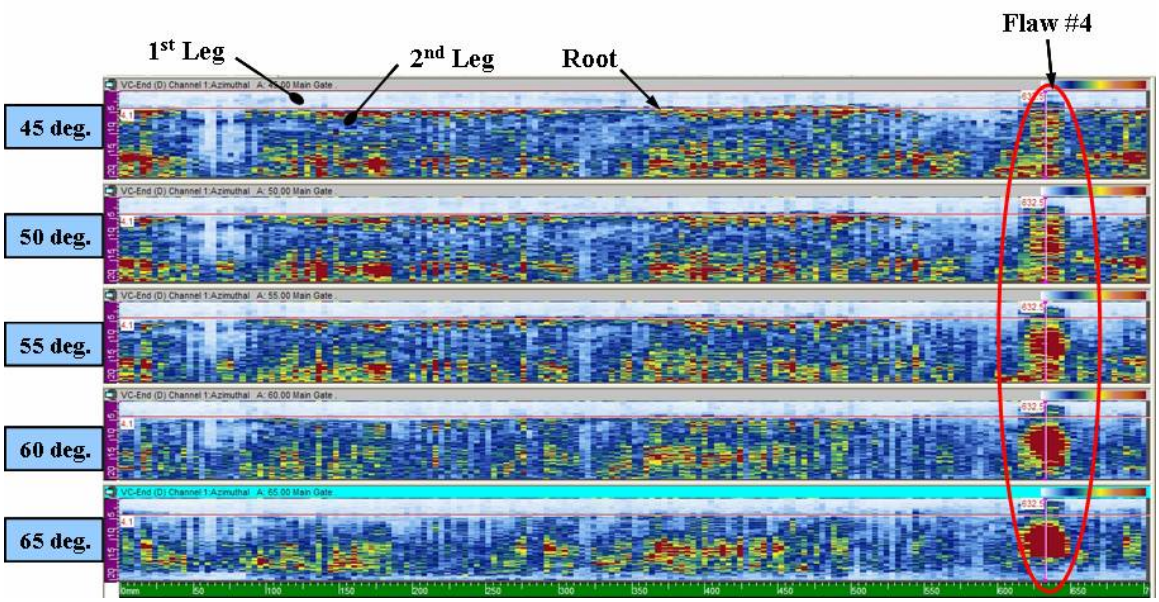

Figure 1.6.3-13. DPA4-24/24 US Scan After Cap Removal

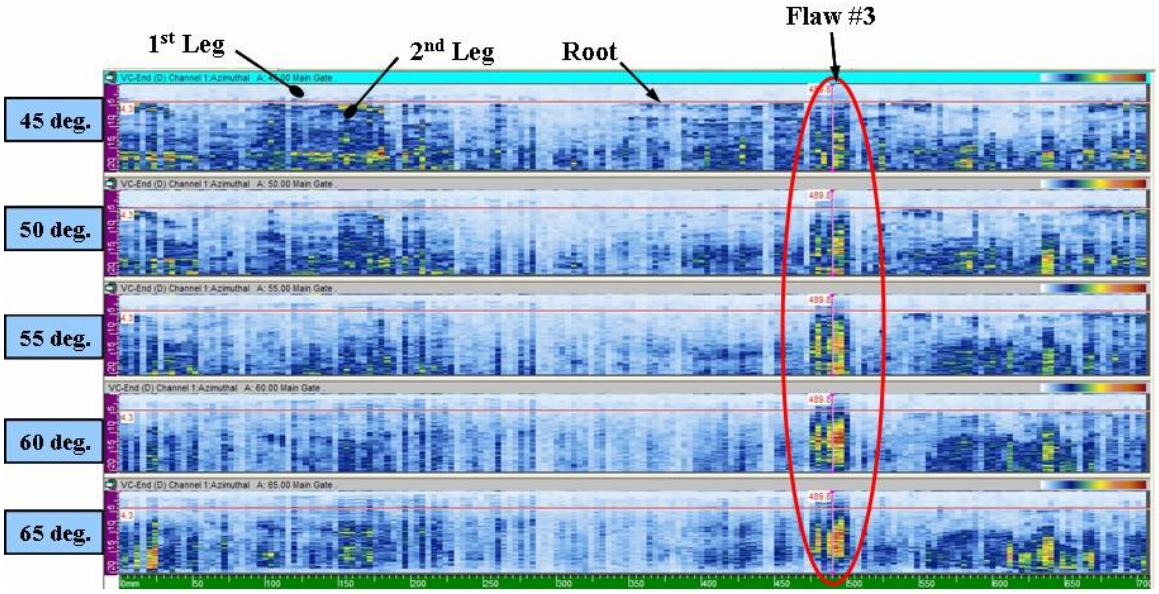

Figure 1.6.3-14. DPA4-24/24 DS Scan After Cap Removal

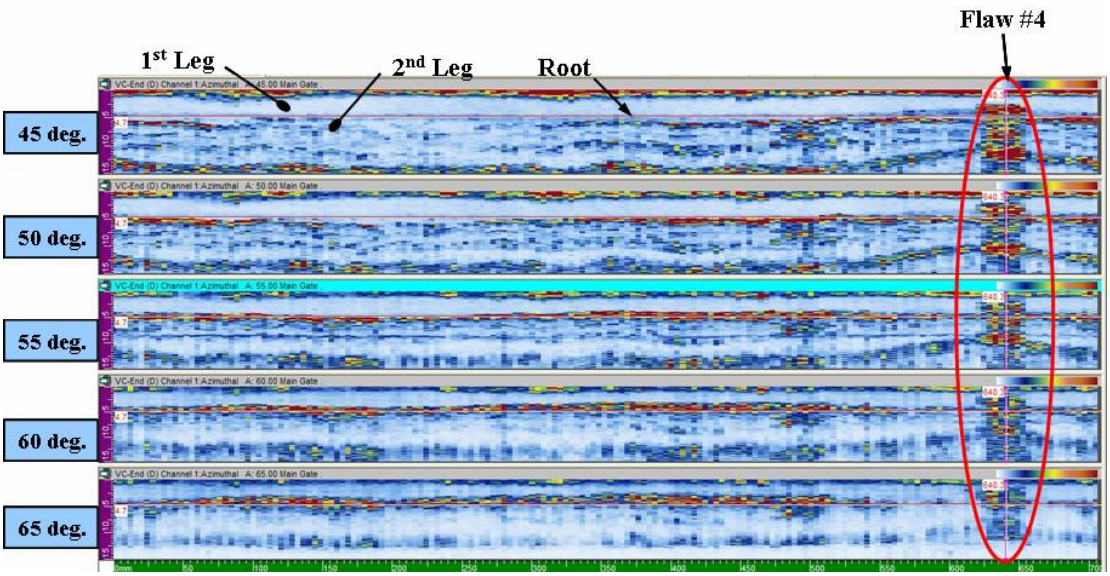

Figure 1.6.3-15. PA10-32/16 US Scan After Cap Removal

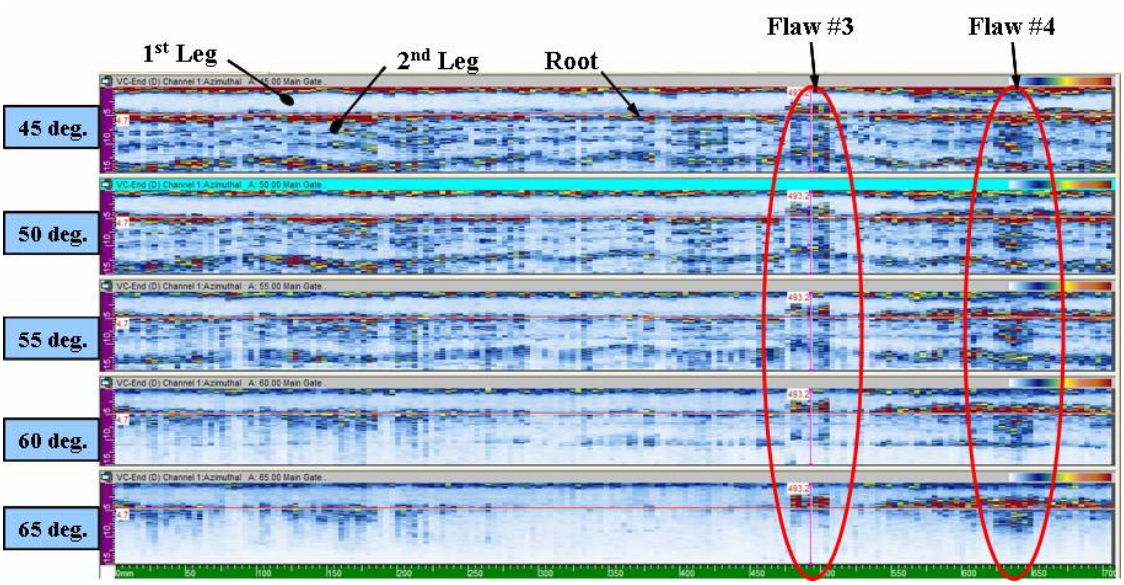

Figure 1.6.3-16. PA10-32/16 DS Scan After Cap Removal

After scanning, all four locations were metallographically cross sectioned near the flaw center to view the flaws. A more detailed analysis of the UT measured flaw height of each flaw was performed using only the PA10-32/16 P/E technique because the DPA4-24/24 technique was found to be better suited for detection than for sizing. A- and S-scan displays for Flaws 3 and 4 are shown in Figures 1.6.3-17 through 1.6.3-21. Metallographic cross sectioning revealed that only Flaws 3 and 4 were present. The intended LOF flaws, 1 and 2, were not found by either metallography or UT. A macro image of each flaw location is shown in Figure 1.6.3-22.

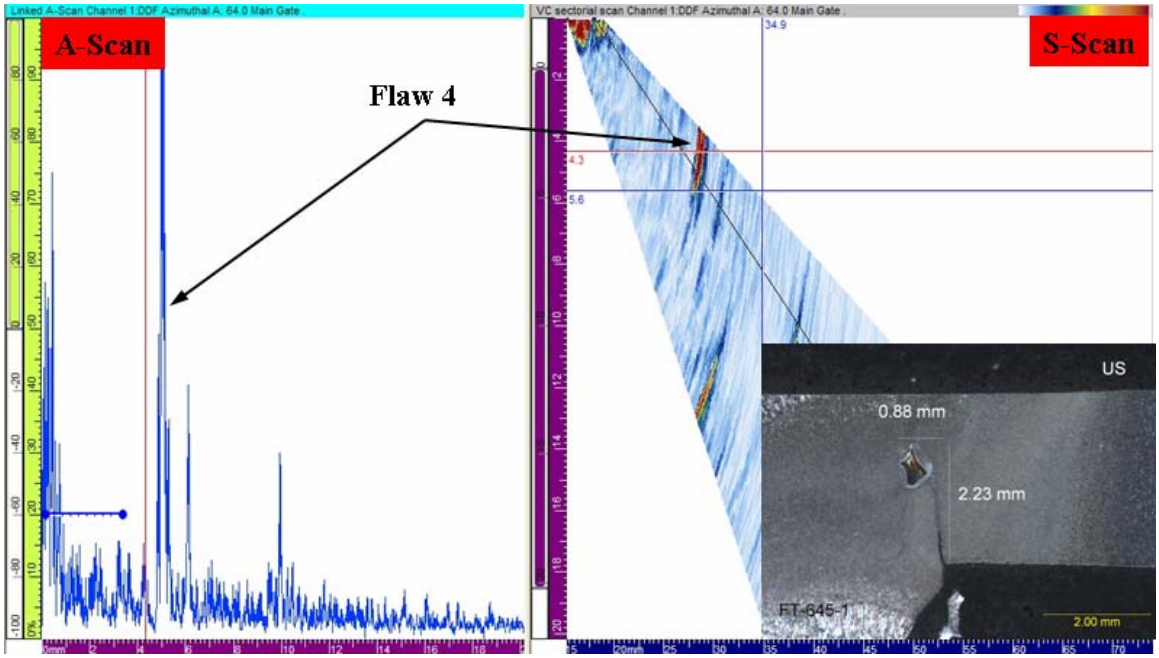

Figure 1.6.3-17. PA10-32/16 US Before Cap Removal

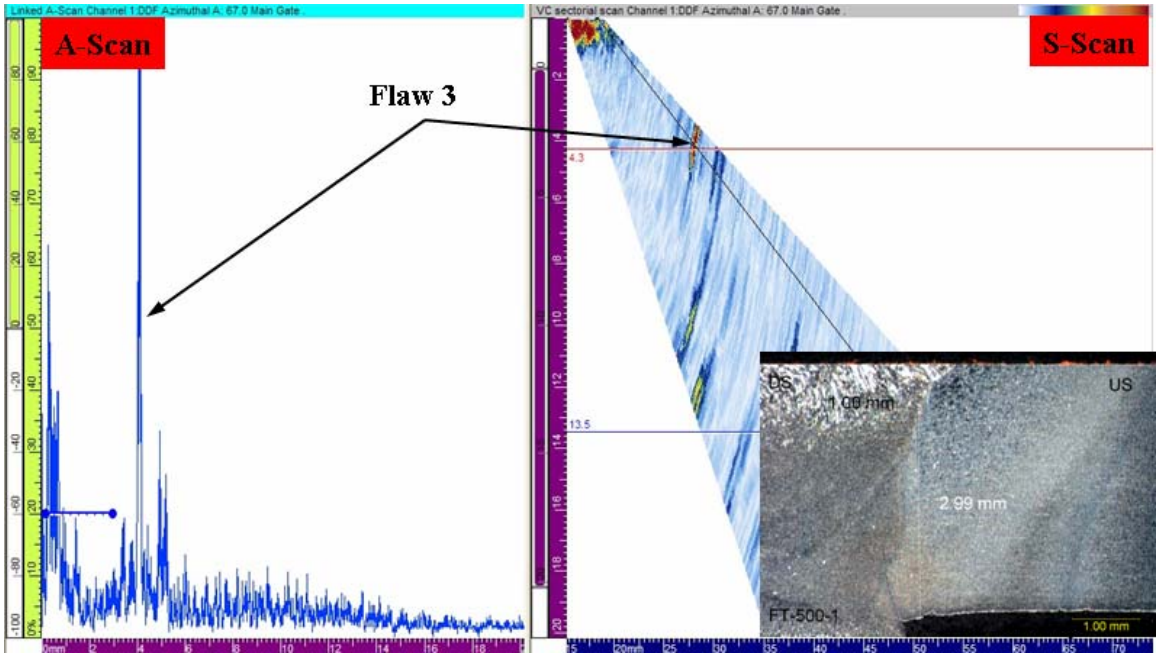

Figure 1.6.3-18. PA10-32/16 DS Before Cap Removal (First Leg)

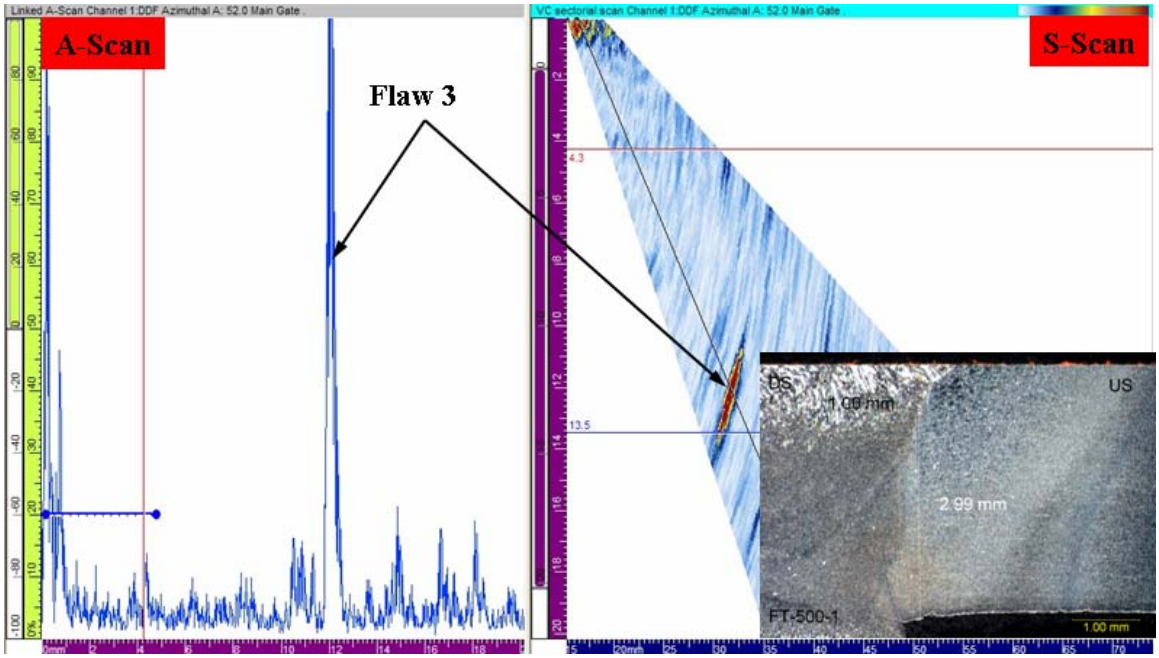

Figure 1.6.3-19. PA10-32/16 DS Before Cap Removal (Third Leg)

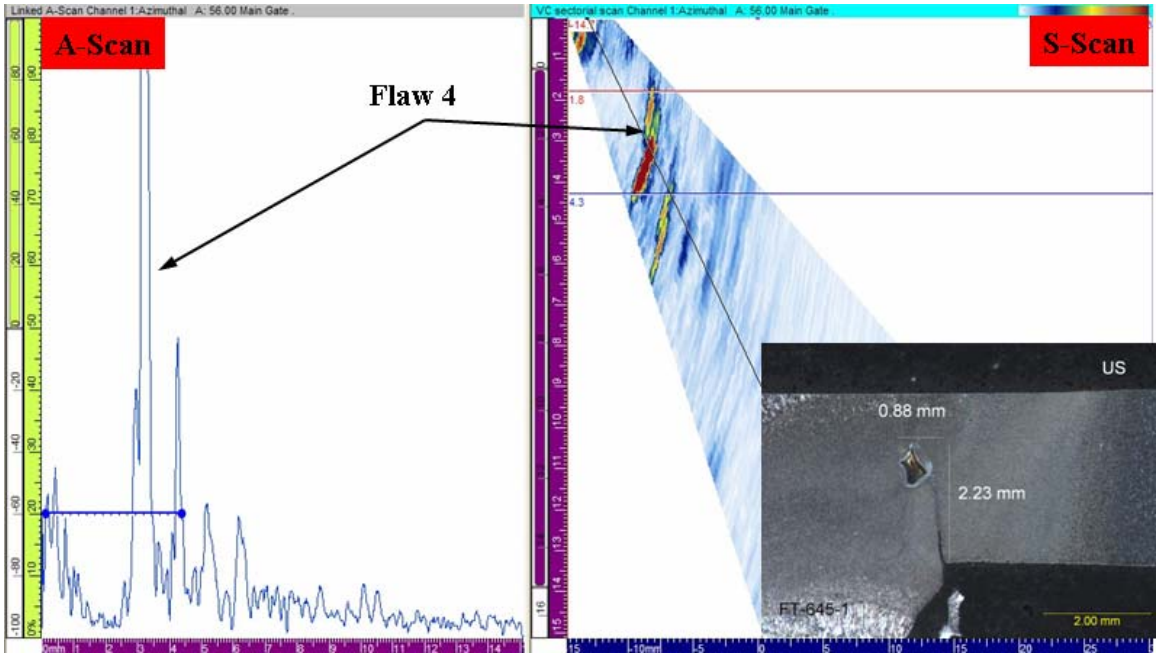

Figure 1.6.3-20. PA10-32/16 US After Cap Removal

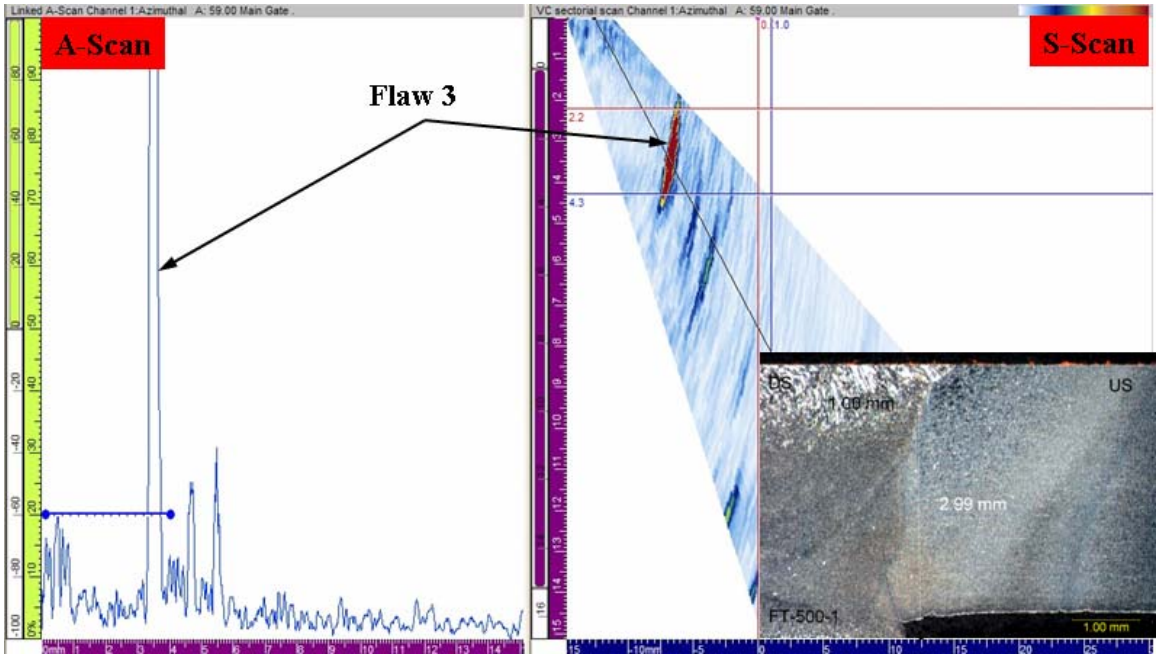

Figure 1.6.3-21. PA10-32/16 DS After Cap Removal

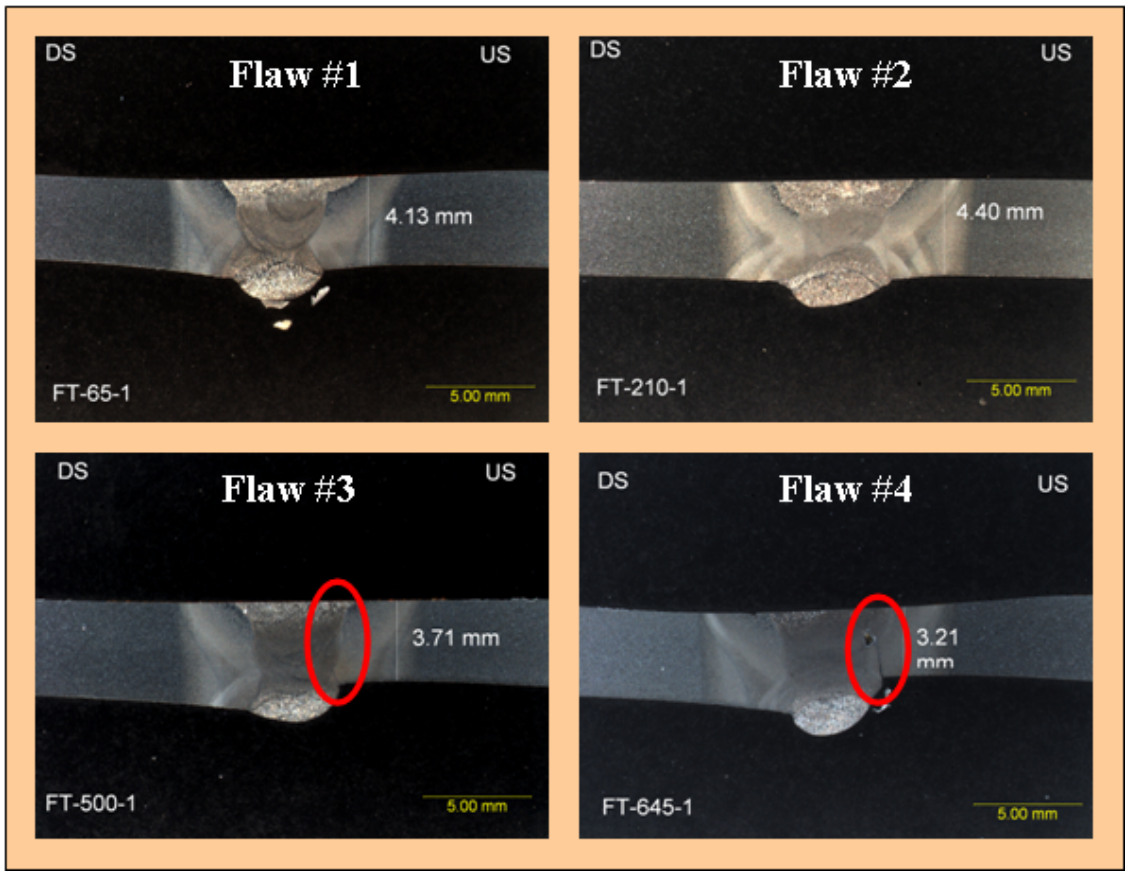

Figure 1.6.3-22. Metallography Results

While both PA techniques detected the flaws well, the PA10-32/16 P/E technique was better suited for determining flaw height. The DPA4-24/24 technique performed very well for flaw detection but was not used for sizing due to multiple sound path possibilities inherent with this type of pitch-catch technique. The noise level was quite high in some scans due to the high scanning gain used in an attempt to detect Flaws 1 and 2 which metallography confirmed were not present.

Mismatch in the pipe fit up and pipe wall thickness variations of approximately 1 mm (0.04 in.) made the ultrasonic evaluation particularly difficult. Despite these difficult challenges, both PA techniques detected the flaws reasonably well even before the weld cap was removed; however, the full extent of the flaw on the first leg could only be imaged after weld cap removal. This can be seen by comparing the S-scan image of Flaw 3 in Figure 1.6.3-18 before cap removal to that in Figure 1.6.3-21 after cap removal. The full extent of Flaw 3 was detected on the third leg before cap removal as shown in Figure 1.6.3-19, but flaw sizing on multiple skips can introduce other uncertainties caused by wall thickness changes and cap/root geometry.

1.6.4 UT Inspection for Service-Induced Fatigue Cracks

Detection and sizing of service-induced fatigue cracks is often challenging because of the narrow crack-tip opening and the smooth face of the fracture surface. When using an angle beam P/E ultrasonic technique, the smooth fracture surface acts as a relatively good acoustical mirror that tends to reflect the ultrasonic sound beam so that very little sound energy is reflected back to the transducer (Figure 1.6.4-1). If the crack is connected to the OD or ID surface, a strong corner trap signal is usually very apparent to help in the detection process; however, cracks with significant through-wall extension can be dramatically undersized using the P/E technique. In addition, mode converted signals may be present that can be mistaken for reflections from the crack (Figure 1.6.4-2). If measurements are made from mode-converted signals, this will lead to inaccurate sizing.

The tandem pitch-catch ultrasonic technique shown in Figure 1.6.4-3 can be effective for detecting fatigue cracks, but it requires the use of several different angle combinations and precise probe spacing to obtain full inspection coverage. The use of pitch-catch for measuring the through-wall extent of fatigue cracks again can require different beam angles and precise probe placement and spacing.

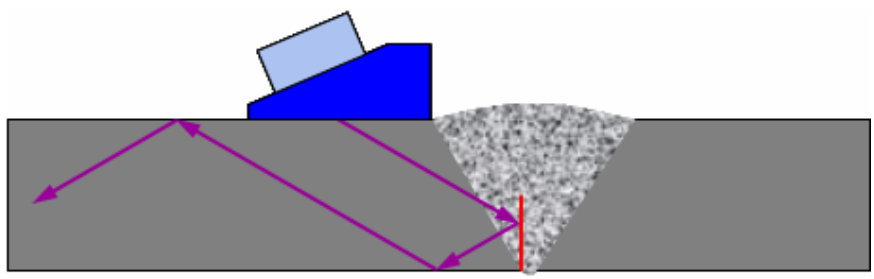

Figure 1.6.4-1. Sound Beam Reflection from the Smooth Face of a Fatigue Crack Using the P/E Technique

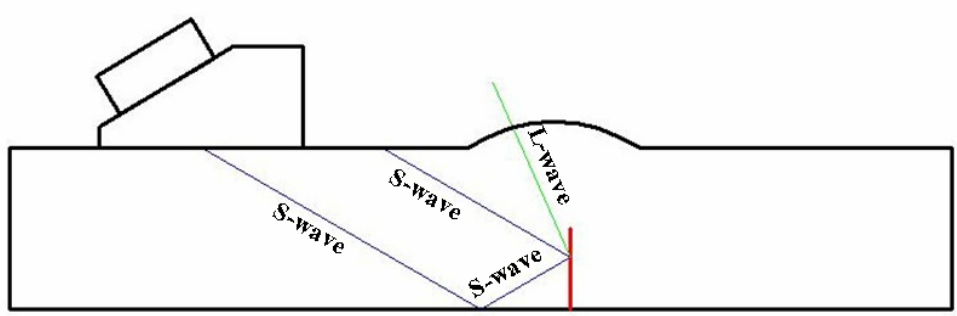

Figure 1.6.4-2. Example of a 60-Degree Shear Wave Mode Converting to an L-Wave After Encountering a Fatigue Crack

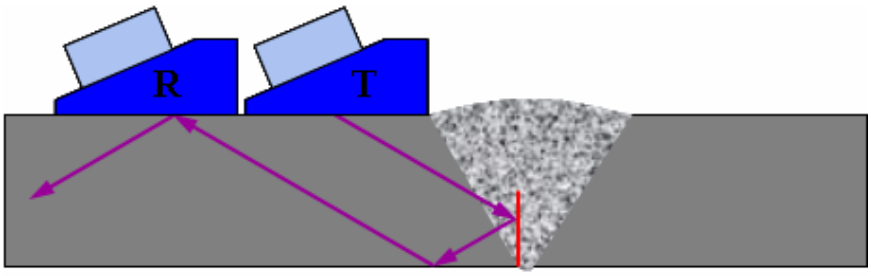

Figure 1.6.4-3. Sound Beam Reflection from the Smooth Face of a Fatigue Crack Using the Tandem Pitch-Catch Technique

During the project pipe sections containing fatigue cracks were scanned using conventional and PA UT. To evaluate the ultrasonic response from fatigue cracks, pipe sections containing fatigue cracks in the weld region, as well as those having fatigue cracks in the base metal were scanned. A variety of beam angles and transducer combinations were used with both the P/E and pitch-catch techniques. Except for the TOFD scans, calibration sensitivity in each case was achieved by adjusting the signal from a 1.2-mm (0.047-in.)-diameter SDH, at a depth of 25.4 mm (1.0 in.) to 80% FSH. Depending on the noise level, an additional 6 to 10 dB was added to the calibration sensitivity level during scanning and data acquisition. The test sensitivity level for TOFD scans was set at the highest gain setting that could be achieved without having excessive signal noise.

1.6.4.1 Fatigue Crack Samples W2 and W3

Fatigue Crack Samples W2 and W3 used for this project were fabricated from 40.6-cm (16-in.)-diameter pipe having a 24-mm (0.94-in.) wall thickness. Both pipes were joined with a J-groove weld. The pipes were subjected to cyclical loading to produce fatigue cracks that propagated from the root to an unknown depth. Because of the welding process used, the root bead was flattened by a backing shoe during welding. This resulted in sharp transitions from the weld metal to the base metal that caused some strong corner reflections during the ultrasonic inspection (Figure 1.6.4-4). Typical root geometry is shown in Figure 1.6.4-5. Three flaws were identified during conventional ultrasonic inspection to be used for more detailed analysis using advanced ultrasonic techniques. The three flaws were identified as W2-1, W3-1 and W3-2. UT and destructive data from Flaw W3-1 was later used for the UT modeling and simulation phase of the project which is reported in Section 1.5.2 of this report.

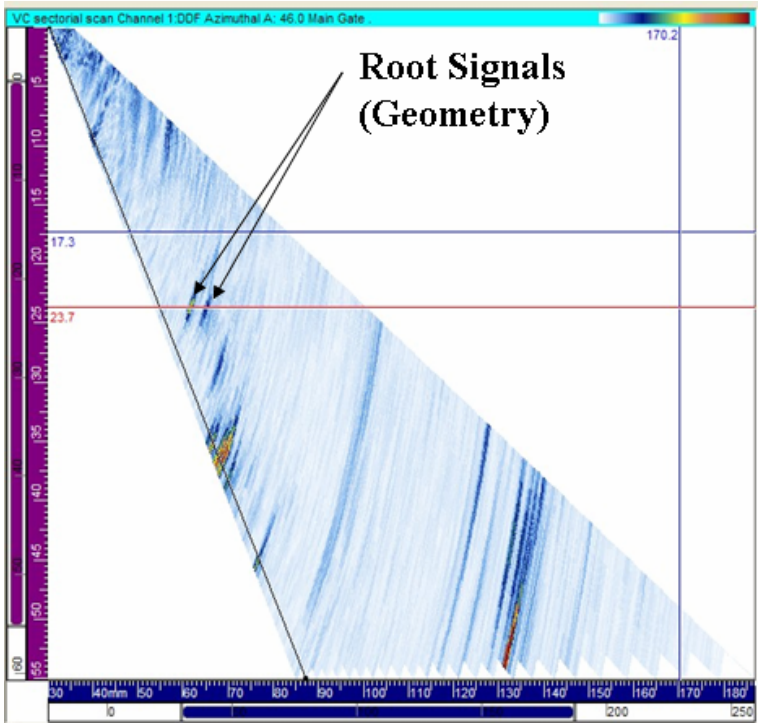

Figure 1.6.4-4. PA Sector Scan Showing Root Signals Caused by Root Geometry

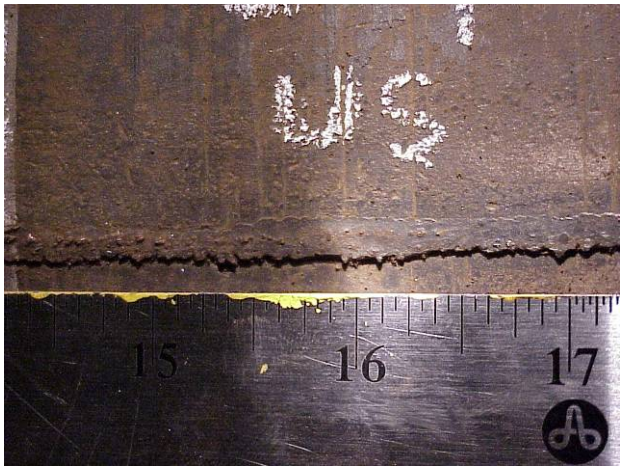

Figure 1.6.4-5. Root Geometry of Weld W3

The three flaw locations were scanned from both the US and DS sides of the weld. Scan data was collected at 2.0-mm (0.08-in.) intervals in the scan direction and 4.0-mm (0.16-in.) intervals in the index direction. For all scans the scan direction was parallel to the pipe axis and the index direction was parallel to the weld. Appendix A1.6.4 contains selected scan images

showing results from the various UT techniques used for scanning Welds W2 and W3. Appendix B1.6.4 shows A- and S-scan images of from data collected using PA techniques.

After scanning Flaw W3-1 an attempt was made to break the sample open to reveal the entire fracture face. The sample was notched on the OD surface to reduce the wall thickness, soaked in liquid nitrogen, and then subjected to a high impact force. This low-temperature fracture technique, however, revealed only a small portion of the crack, so metallographic cross sectioning was used to view the crack height at several locations along the crack length. The metallographic cross sections were performed every 1 to 1.5 mm (0.04 to 0.06 in.) along the length of the flaw and revealed what appeared to be a straight fatigue portion of the crack and a jagged brittle fracture extending from the fatigue crack (Figure 1.6.4-6). It was theorized that the brittle fracture extension was caused by the unsuccessful low-temperature fracture. This was supported by the absence of the jagged brittle fracture portion on subsequent cross sections of Flaws W2-1 and W3-2. Consequently, the fatigue portion and the brittle fracture extension were measured separately and the results were compared to the UT data.

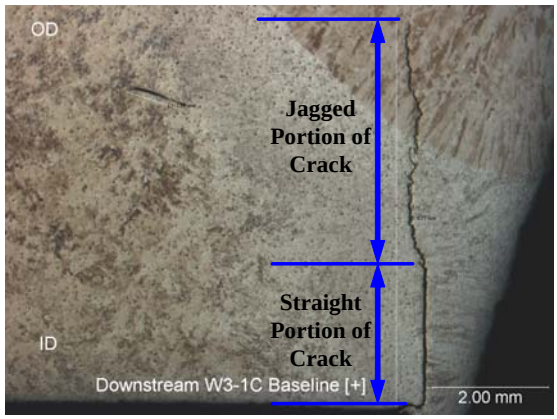

Figure 1.6.4-6. Crack W3-1 Showing Straight and Jagged Fracture Profiles

Figure 1.6.4-7 shows a comparison of the destructive data to the UT data obtained with a PA7-60/17 technique. The sharp root transition made the UT results difficult to interpret due to the strong reflected signal coming from the root geometry. Even with the focused PA beam the strong root signal effectively masked any root flaw less than 1.5 to 2 mm. This was also the case for the TOFD scan shown in Figure 1.6.4-8 where crack heights less than approximately 1.5 mm could not be resolved from the back surface signal. Flaws that were greater than approximately 2 mm in height could be separated from the background root signals. While it was difficult to separate noise relevant signals from non-relevant signals on the A-scan display, the use of other data imaging views as shown in Figure 1.6.4-9 such as B-, C-, D-, and S-scans helped reveal crack locations and height.

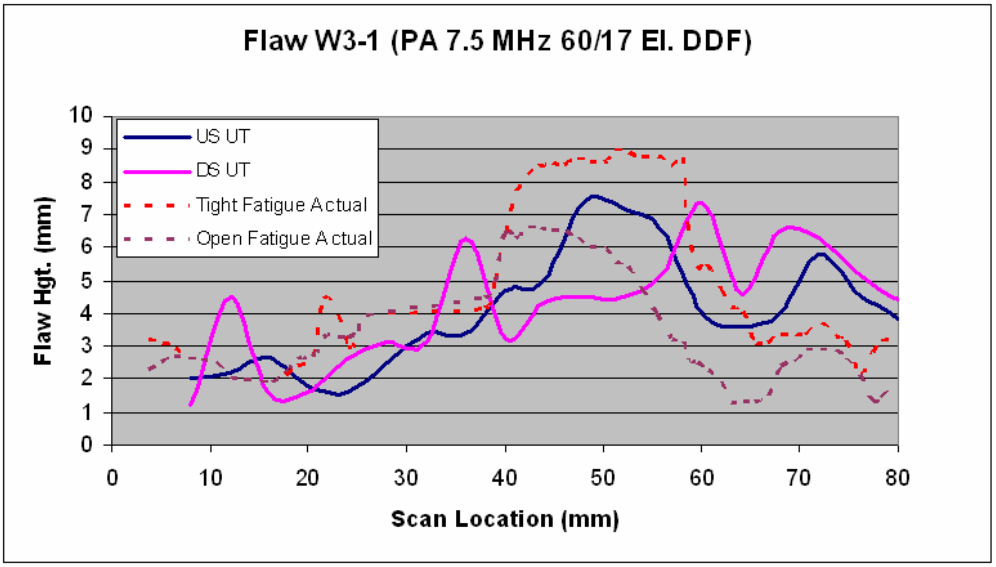

Figure 1.6.4-7. Flaw W3-1; UT Flaw Height Comparison to Metallographic Data

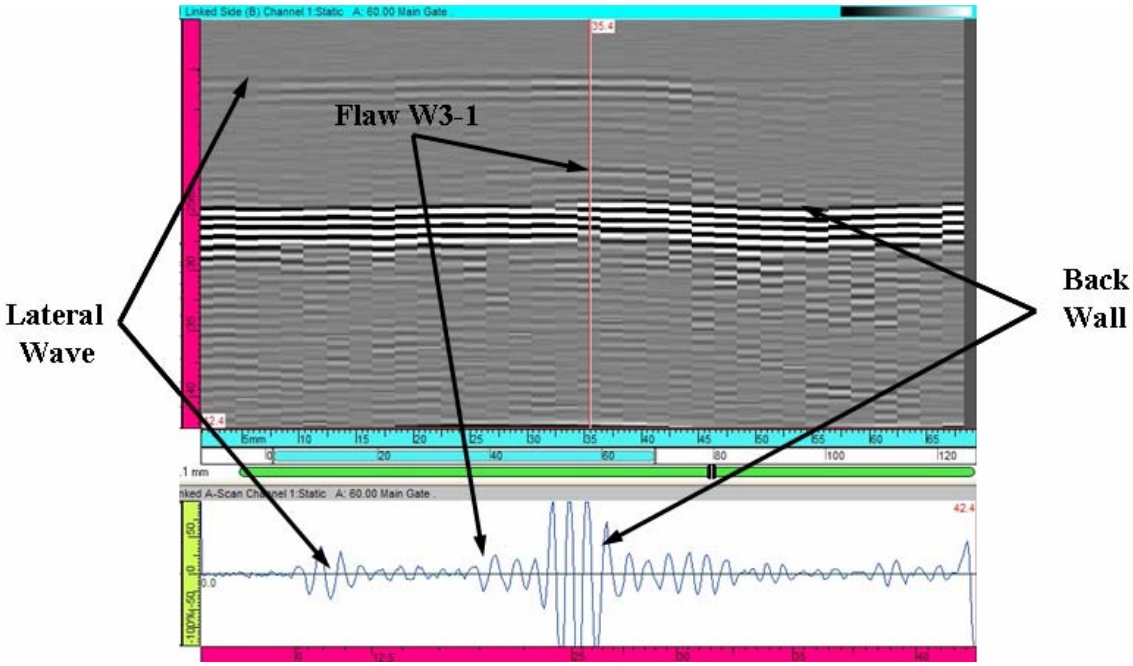

Figure 1.6.4-8. TOFD Scan Data from Flaw W3-1

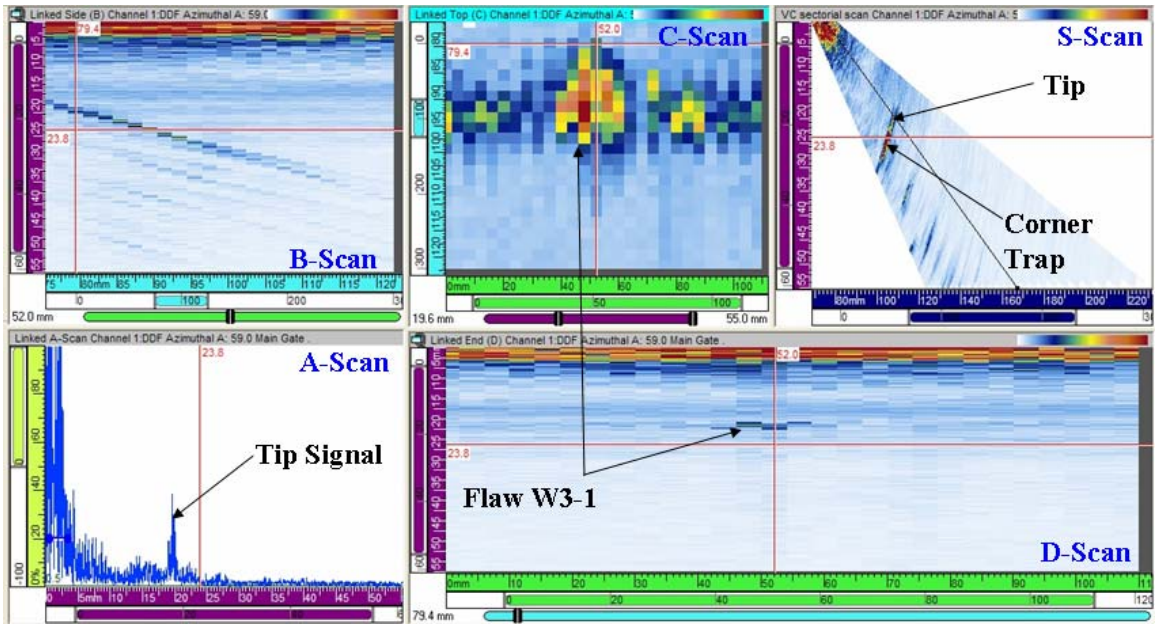

Figure 1.6.4-9. Use of A-, B-, C-, D-, and S-scans to Visualize Flaw W3-1

Because of the unsuccessful attempt in breaking open Flaws W3-1, W2-1, and W3-2 were cross sectioned along the flaw length to reveal the crack height. Figures 1.6.4-10 through 1.6.4-12 show the UT results for multiple techniques compared to the metallography cross section measurements for each of the three flaws. Due to a combination of insufficient scan surface distance and probe size, the PA4-64/32 upstream scan could not be performed on Flaw W2-1. Also, PA4-64/32 scans were not performed on Flaw W3-1.

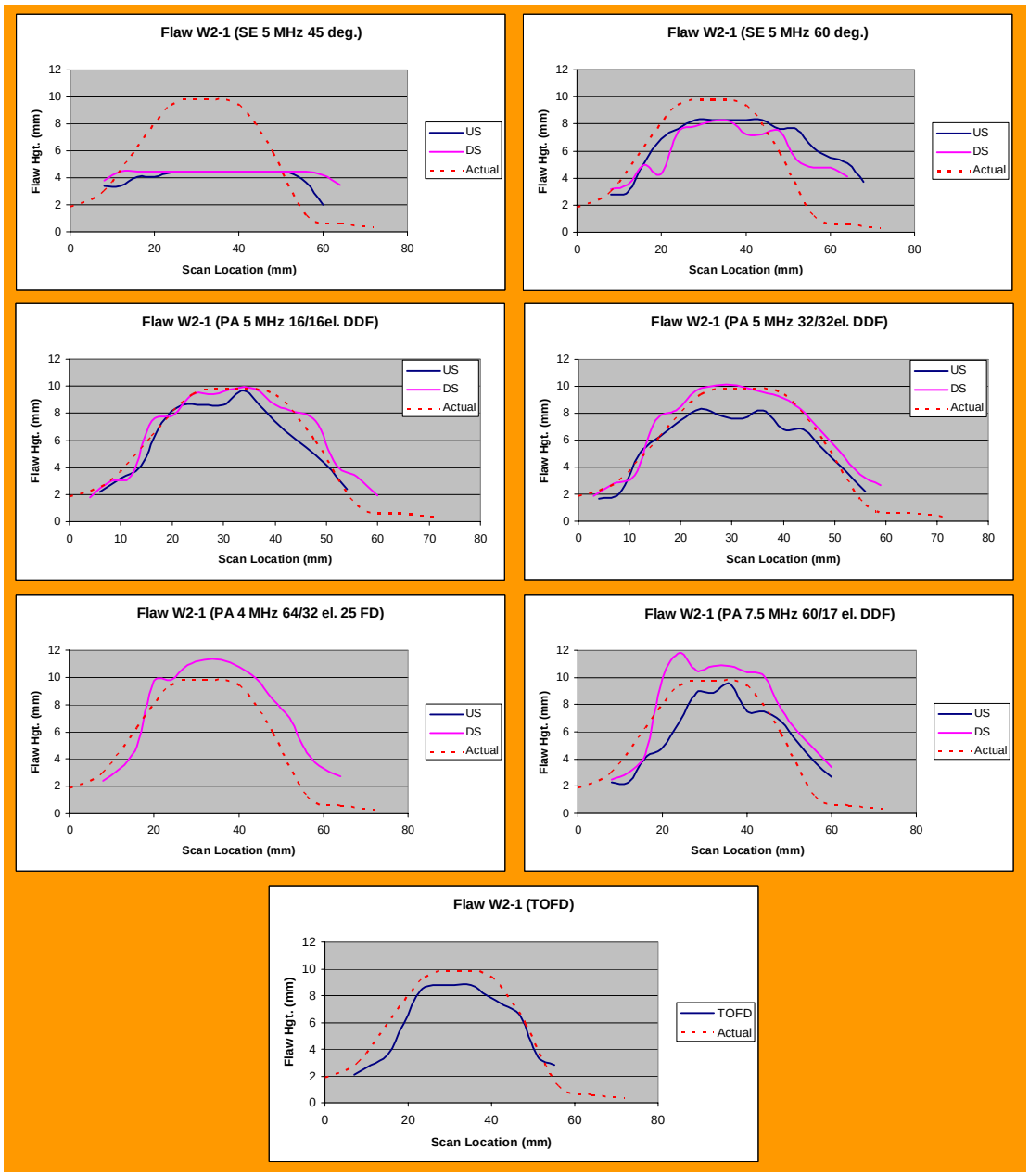

Figure 1.6.4-10. Flaw W2-1; UT Flaw Height versus Actual Flaw Height

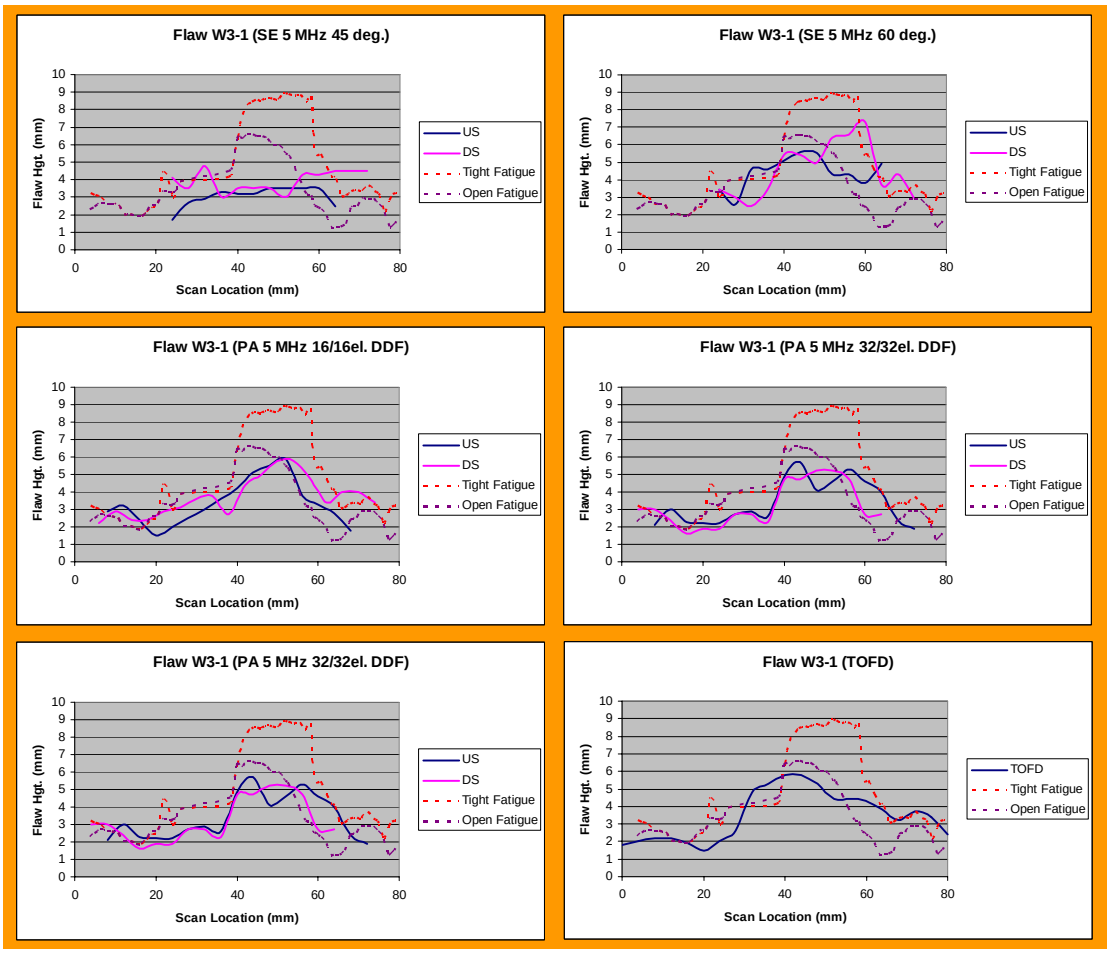

Figure 1.6.4-11. Flaw W3-1; UT Flaw Height versus Actual Flaw Height

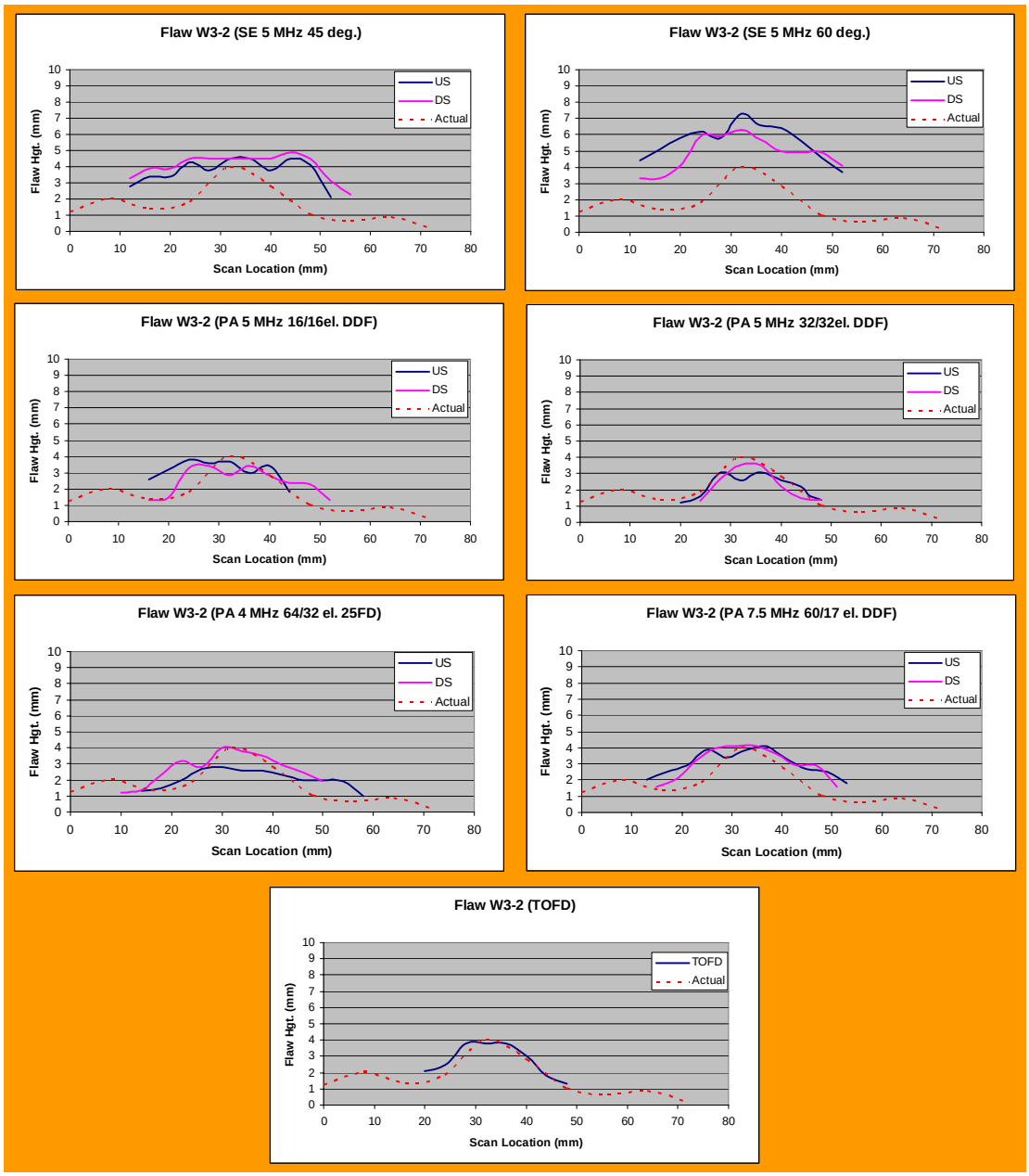

Figure 1.6.4-12. Flaw W3-2; UT Flaw Height versus Actual Flaw Height

Results for Flaws W2-1 and W3-2 showed that greater sizing accuracy was achieved using PA techniques and TOFD than when using conventional SE probe techniques. The SE5-45-degree probe detected only the echo-dynamic of the corner trap signal resulting in a constant flaw height of between 4 and 5 mm regardless of the actual flaw height. When using a SE5-60-degree probe the flaws was sized within approximately 2 mm when a tip signal was detected; however, tip signals were typically not detected by the SE5-60 probe when the crack height was less than about 3 to 4 mm. The chevron profile of these fatigue cracks and the tight crack tips are possible explanations for the fact that there was little or no tip signal detected.

There was considerable scatter in the data for Flaw W3-1, which was likely caused by inaccuracies in the destructive cross section measurements stemming from problems previously noted. Consequently, destructive data for Flaws W2-1 and W3-2 should be considered the most reliable data. Based on comparisons of the destructive results with the UT results, UT techniques having smaller beam dimensions such as the PA techniques were more accurate than those having larger beams such as the single-element techniques. The TOFD technique also performed well despite the low amplitude of the received signals and a S/N ratio of approximately 2:1. PA techniques also provided another benefit. By measuring the vertical extent of a flaw on the PA sector scan, a good estimate of flaw height could be determined even when a tip signal was not detected.

Through-Wall Base Metal Fatigue Crack, Sample W302-2

Sample, W302-2, was a 272-mm (10.7-in.)-diameter pipe having an 11.7-mm (0.460-in.) nominal wall thickness. The flaw in Sample W302-2 was a through-wall base metal fatigue crack. Sample W303-2 is shown in Figure 1.6.4-13.

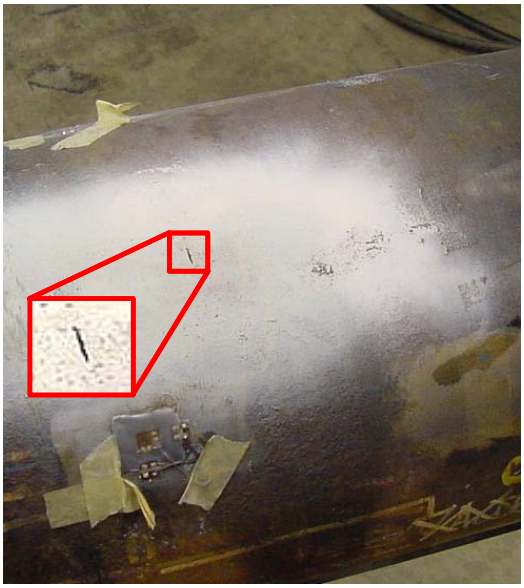

Figure 1.6.4-13. Sample W302-2 Showing OD Crack as Detected by Magnetic Particle Inspection

The crack location of the pipe was scanned from both the US and DS sides of the crack except for the PA7-60/17 and PA7-60/17T-17R techniques which were scanned only from the DS side of the crack. Scan data was collected at 2.0-mm (0.08-in.) intervals in the scan direction and 4.0-mm (0.16-in.) intervals in the index direction. For all scans the scan direction was parallel to the pipe axis and the index direction was parallel to the pipe circumference. Appendix C1.6.4 contains selected scan images showing results from the various UT techniques used for scanning the crack location.

A post-processing data merge was performed on scan data from each technique to help in detection of the through-wall crack. The data merge process was accomplished by taking data from each angle of the sector scan, as well as each scan and index location and combining it into a single file with all the data corrected for location and angle. This proved to be a very useful tool for visualizing the cross sectional dimensions of the through-wall fatigue crack in this sample and for evaluating the ability of each technique to detect the crack.

In general, all techniques detected the crack very well; however, the lower angles (45 to 50 degrees) generally detected only the ID and OD corner trap effect. For example, Figure 1.6.4-14 shows the ID response and Figure 1.6.4-15 shows the OD response from the through-wall crack when using the P/E SE5-45 technique. While the corner trap signals were distinct there was little or no reflected signal from the crack face to indicate a through-wall crack. This was especially evident when comparing the merged D-Scan image of the 45-degree shear wave to that of the 60-degree shear wave in Figures 1.6.4-16 and 1.6.4-17. Although the ID and OD

corner trap signals from the 60-degree shear wave shown in Figures 1.6.4-18 and 1.6.4-19 were weaker than those at 45 degrees, the reflected energy from the crack face at 60 degrees helped to identify the flaw as a through-wall crack.

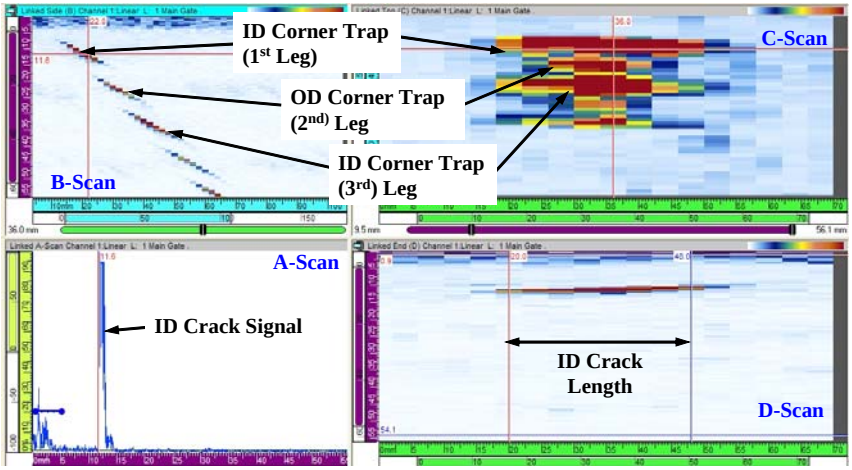

Figure 1.6.4-14. ID Corner Trap Signal from W302-2 Through-Wall Base Metal Crack When Using the P/E SE5-45 Technique

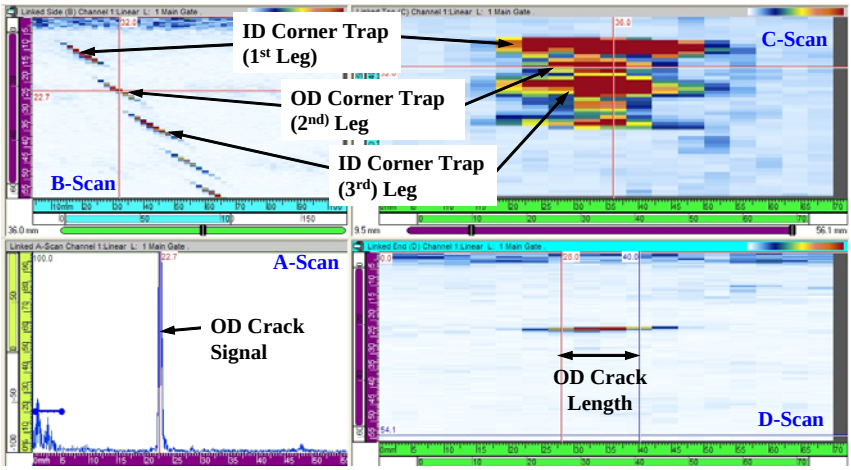

Figure 1.6.4-15. OD Corner Trap Signal from W302-2 Through-Wall Base Metal Crack When Using the P/E SE5-45 Technique

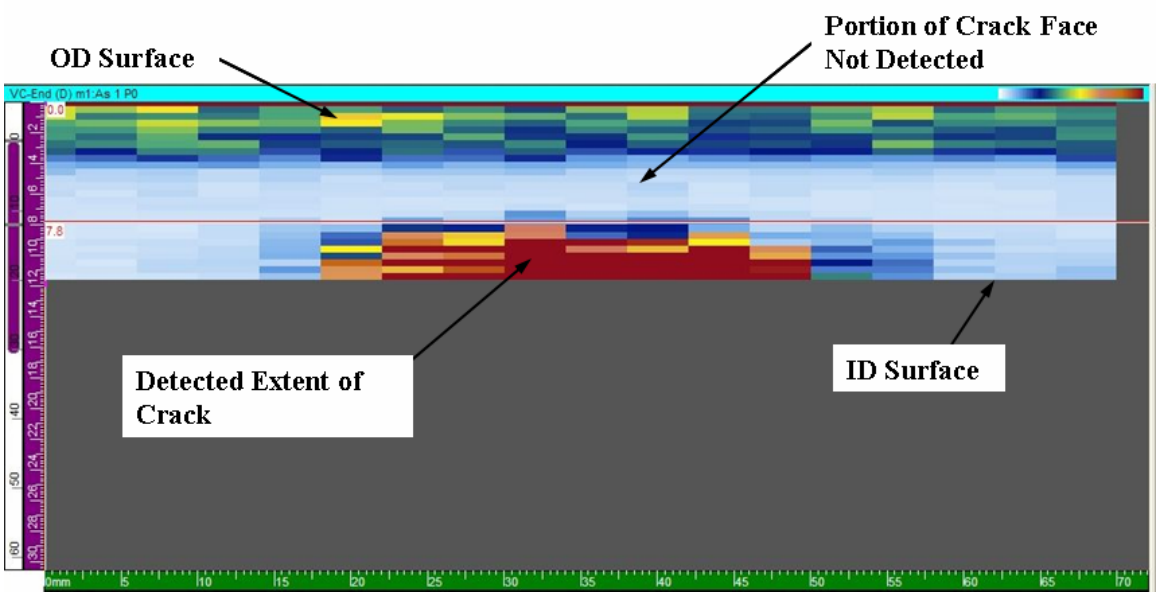

Figure 1.6.4-16. Merged D-Scan View of W302-2 Through-Wall Base Metal Crack When Using the P/E SE5-45 Technique

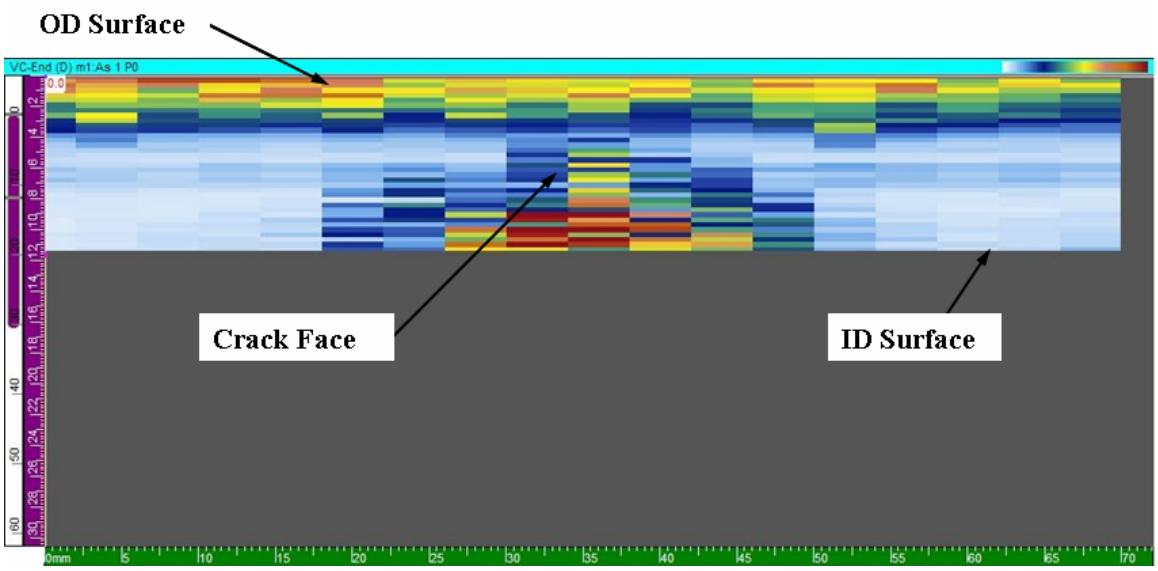

Figure 1.6.4-17. Merged D-Scan View of W302-2 Through-Wall Base Metal Crack When Using the P/E SE5-60 Technique

Another interesting phenomenon occurred when using higher refracted angles. At a refracted inspection angle of 60 degrees the shear wave mode converted when hitting the crack face resulting in a compression wave (L-wave) which appeared to bounce off the OD surface of the pipe. The L-wave travels at approximately twice the velocity of the shear wave which led to

multiple signals appearing after the ID corner trap on the A-scan display. These mode converted signals can be seen in Figure 1.6.4-18. Although the mode converted signals could not be used in this case for flaw sizing purposes they did provide a good indicator that the crack was approximately vertical and/or the crack had significant through-wall height. The sketch in Figure 1.6.4-2 shows how a 60-degree shear wave can mode convert and reflect from the OD surface.

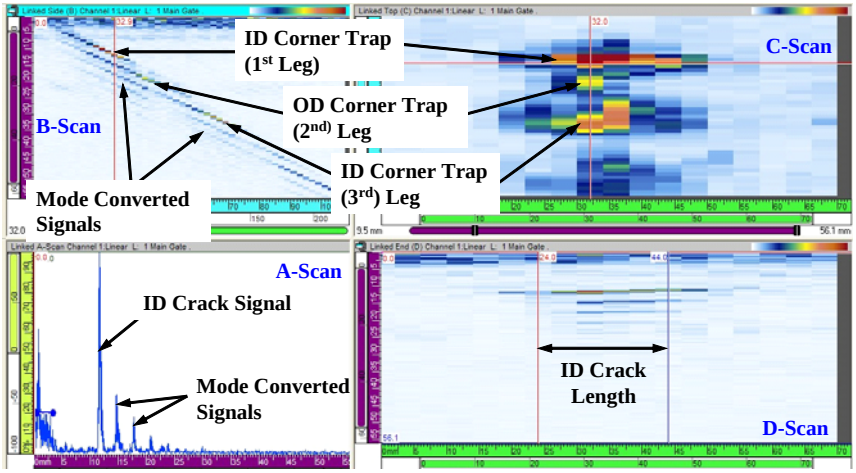

Figure 1.6.4-18. ID Corner Trap Signal from W302-2 Through-Wall Base Metal Crack When Using the P/E SE5-60 Technique

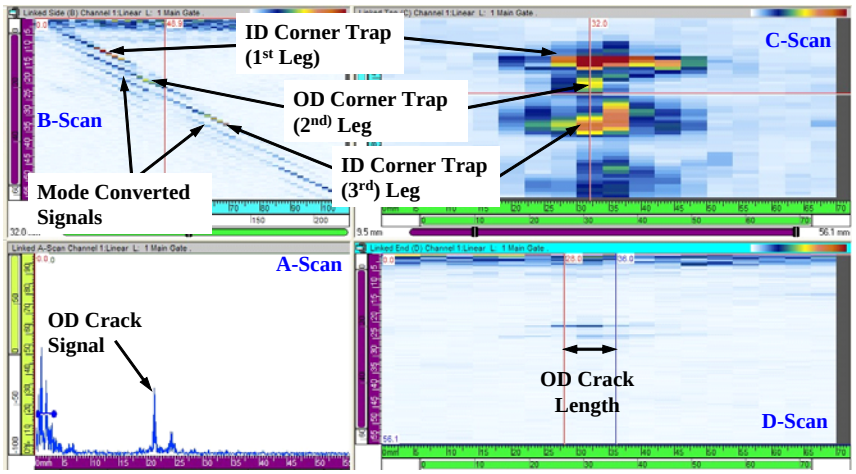

Figure 1.6.4-19. OD Corner Trap Signal from W302-2 Through-Wall Base Metal Crack When Using the P/E SE5-60 Technique

Since pitch-catch techniques usually work well for detecting planar flaws lying in the through-wall plane, two pitch-catch techniques were tried for Flaw W302-2. Both techniques used PA probes. The first was a tandem arrangement using different element groupings of a linear PA

probe for transmitting and receiving. The transmit and receive angles and the distance between active element groupings were calculated to detect vertical flaws near mid-wall. The second pitch-catch technique used was a dual-PA probe arrangement where two PA probes were mounted side by side on a wedge having a 6-degree roof angle. This roof angle was necessary in order to provide some focusing of the beam in the passive (secondary) axis. Both probes in the dual-PA arrangement were 4-MHz, 24-element probes (DPA4-24/24). One probe transmitted the sound wave and the other probe received. Unlike the fixed angles of the tandem technique, the dual-PA probes were electronically steered in the active (primary) axis to sweep through a range of angles from 45 to 70 degrees.

Tandem pitch-catch scans were performed on Sample W302-2 using a single PA 7.5 MHz 60-element probe with the technique identified as PA7-60/17T-17R for this report. The PA7-60/17T-17R pitch-catch technique consisted of a group of 17 elements transmitting at a shear wave angle of 45 degrees and a group of 17 elements receiving at a shear wave angle of 55 degrees. Figure 1.6.4-20 shows the scan results for this tandem pitch-catch technique. As Figure 1.6.4-20 shows, more reflected sound energy was received from the crack face when using the tandem pitch-catch technique than when using conventional P/E techniques. Since more reflected sound energy was received with the tandem technique, the crack face was much more apparent. The merged D-scan view in Figure 1.6.4-21 shows that the tandem technique provides good detection of the crack face.

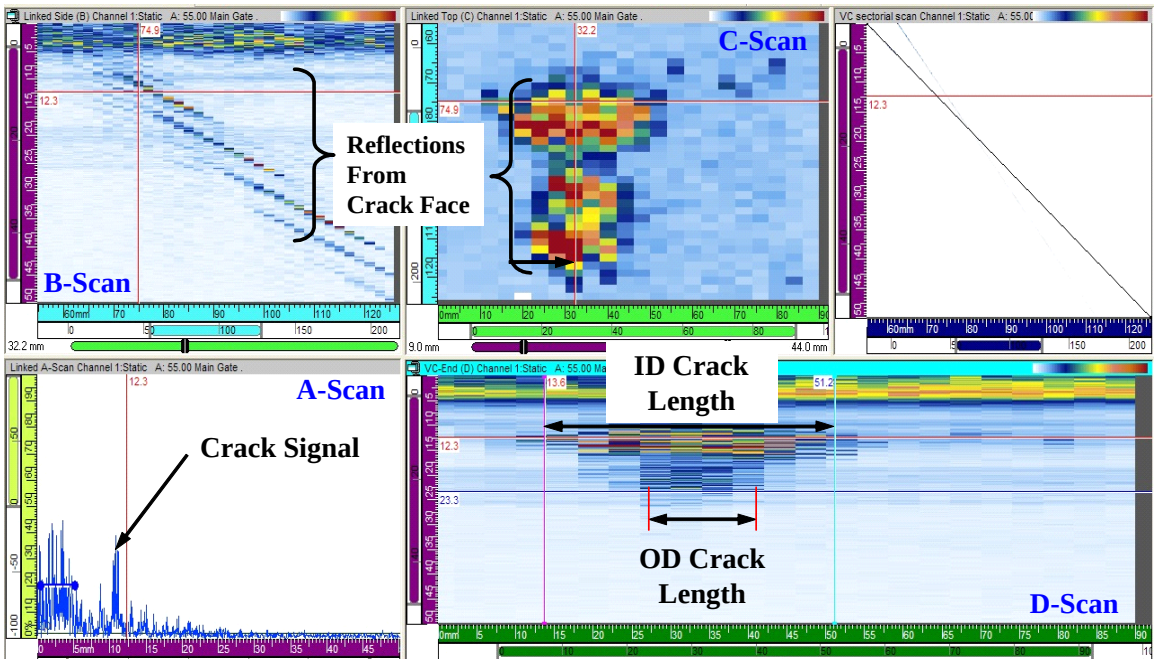

Figure 1.6.4-20. Scan Results Using the PA7-60/17T-17R Tandem Technique on Flaw W302-2

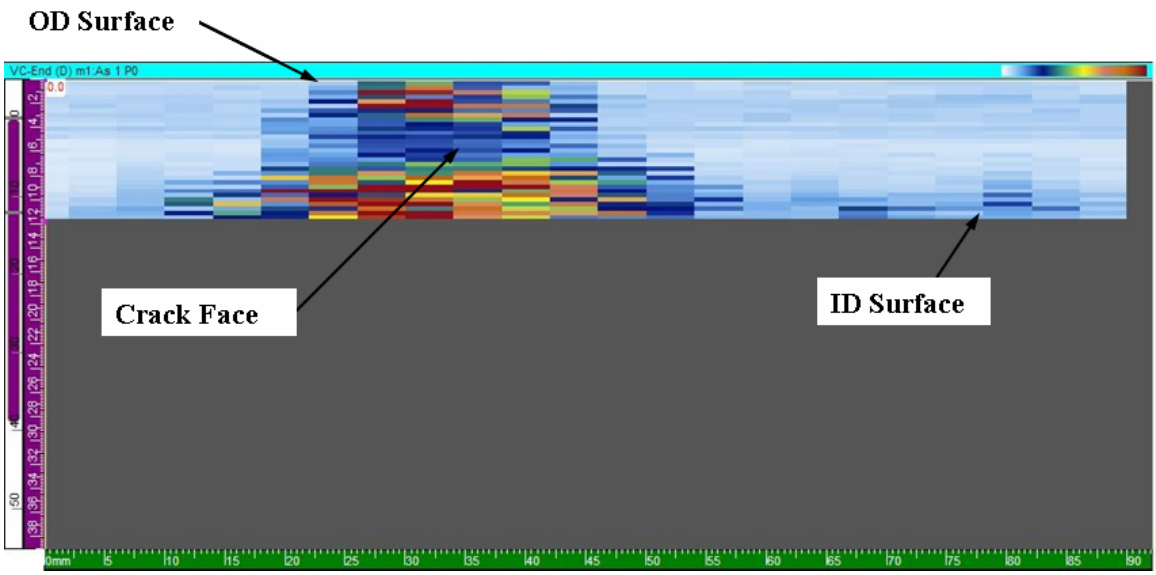

Figure 1.6.4-21. Merged D-Scan View of W302-2 Through-Wall Base Metal Crack When Using the PA 7-MHz Tandem Pitch-Catch Technique

Data from the dual-PA technique proved to be somewhat difficult to interpret due to multiple paths that a sound beam can take from the transmitter to the receiver when using sector scanning. For example, the sound beam could reflect directly from the crack face on the first leg and be received on the first leg; or the same transmitted beam could be received by another angle after it had bounced off the back wall. Mode conversions and other sound path possibilities resulted in the same flaw being seen at different positions on the sector scan as shown in Figure 1.6.4-22. It was found that merging the dual-PA data helped in the interpretation and visualization of the actual flaw. Consequently, the dual-PA data was merged and displayed as a merged D-scan (Figure 1.6.4-23). The DPA technique had a low noise level and proved very good for detecting the extent of through-wall crack W302-2; however, because of multiple sound paths and mode conversions, through-wall sizing was not as good as other techniques. Although through-wall sizing was problematic, lateral focusing by means of the wedge roof angle, reduced the affects of lateral beam spread in the passive axis which, in turn, improved the capabilities for measuring crack length.

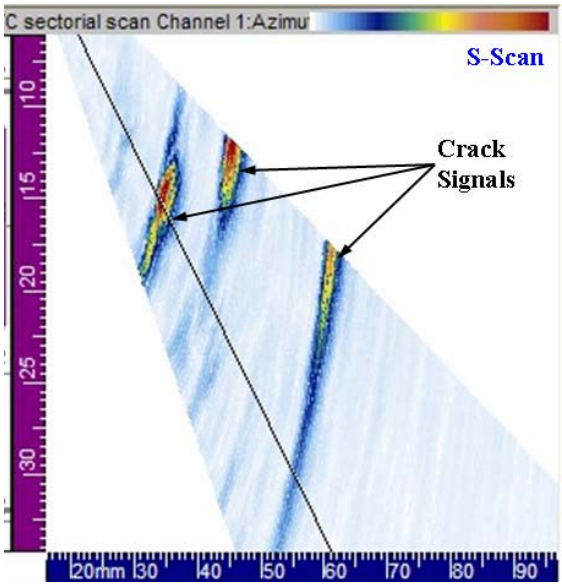

Figure 1.6.4-22. Multiple Signals from a Single Crack Using the Dual-PA Technique

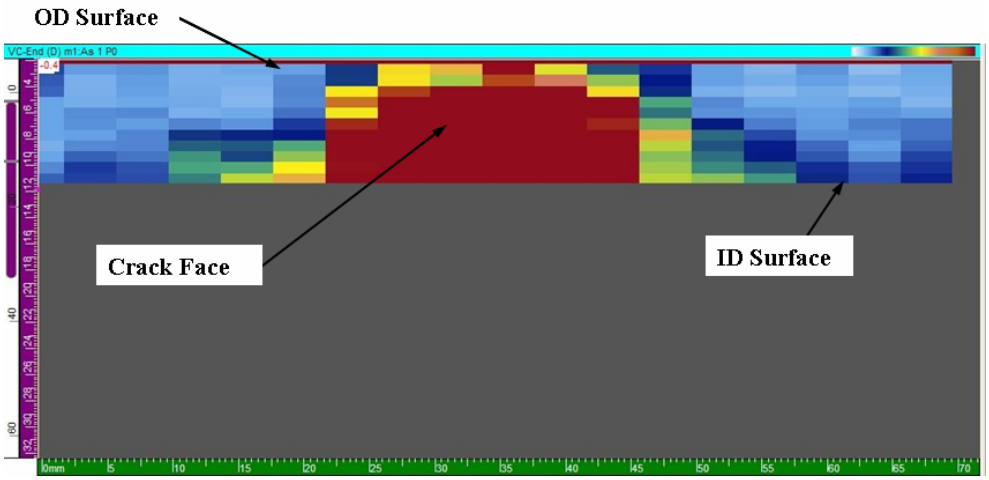

Figure 1.6.4-23. Merged D-Scan View of W302-2 Through-Wall Base Metal Crack When Using the Dual-PA 4-MHz Pitch-Catch Technique

While good detection of the crack face was achieved using the pitch-catch techniques, it was found that the extent of the crack could also be determined by merging sector scan data from P/E PA techniques. In fact, after merging the multiple angle data obtained by electronically steering the beam from 45 to 70 degrees, it was found that detection of the crack face was very similar to that achieved using the dual-PA technique. Merged D-scan views of the dual-PA pitch-catch and single PA probe (PA7-17/60) P/E techniques are shown in Figures 1.6.4-23 and 1.6.4-24, respectively.

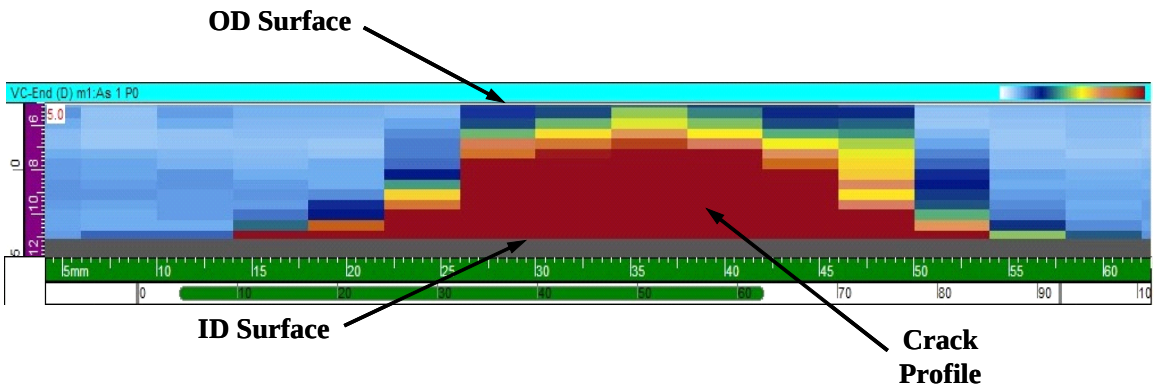

Figure 1.6.4-24. View of Merged Angle Data (45 to 70 Degrees) for Flaw W302-2 Using PA7-60/17 P/E Technique

Based on experimental results from surface-breaking fatigue cracks in material up to 25 mm (1.0 in.) in thickness and with cracks having different through-wall heights, the following observations were made:

- Good detection of the corner trap from the cracks was achieved using P/E techniques with shear wave beam angles in the range of 45 to 50 degrees and a probe frequency in the range of 4 to 10 MHz. These angles, however, were not good for determining the through-wall height of the cracks.

- The best detection of the crack face on through-wall cracks was achieved using tandem pitch-catch and dual-PA pitch-catch techniques. These techniques provided the best detection with the lowest noise level.

- Good through-wall sizing was obtained using shear wave beam angles in the range of 50 to 70 degrees and a probe frequency in the range of 4 to 10 MHz. Single-element and PA techniques were both useful for sizing provided a crack tip signal could be detected.

- UT P/E techniques having small beam sizes in the through-wall dimension had consistently better sizing accuracy.

- Fatigue cracks less than 1.5 mm (0.06 in.) in height were difficult to size because the relatively weak crack tip signal was usually not fully resolved from the strong corner trap signal and root geometry echoes.

- Even with relatively high gain settings during scanning, crack faces, and crack tips from the fatigue cracks were difficult to detect.

- PA P/E techniques worked well for crack sizing when using the sector scan technique to electronically steer the sound beam through a range of angles. Even when a tip signal could not be detected, the sector scan display gave a good estimate of the through-wall extension of the cracks.

- TOFD was only tried on ID connected cracks having through-wall extensions less than 50%. However, in these cases, TOFD worked very well for sizing fatigue cracks when a good diffracted signal was received. Because of the low S/N ratio it was sometimes difficult to resolve the diffracted signal from the crack in these experiments.

- The use of data merging techniques proved very useful for visualizing the through-wall extent of cracks, as well as the crack length.